NPL Report CMSC 11/01

# The Application of Wavelets and Other Techniques to the Calibration of Underwater Electroacoustic Transducers in Reverberant Laboratory Tanks

P M Harris, G J Lord, I M Smith
and S P Robinson

**September 2001**

# The Application of Wavelets and Other Techniques to the Calibration of Underwater Electroacoustic Transducers in Reverberant Laboratory Tanks

Peter M Harris, Gabriel J Lord and Ian M Smith
Centre for Mathematics and Scientific Computing

and

Stephen P Robinson
Centre for Mechanical and Acoustical Metrology

September 2001

## ABSTRACT

In the calibration of underwater electroacoustic transducers undertaken in reverberant laboratory tanks, data processing is used to extract from the measured data the required information for the calibration. This information is the voltage that would be measured in the absence of contaminating effects, including transients due to the resonances of the devices, reflections of the transmitted signal, and noise.

There are a number of approaches to performing the data analysis currently in use, including the application of signal processing techniques based on Fourier analysis as well as regression modelling. Wavelet analysis provides another approach to analysing spectrally varying sequences of data that complements the traditional Fourier analysis. Wavelets provide a general set of basis functions that are localised both in time and frequency, and wavelet analysis has been applied successfully to problems in feature recognition, signal compression, function representation and as a basis for numerical schemes. The coefficients obtained in a wavelet expansion are useful as they relate directly to a time (or place) and frequency, and to the smoothness of the signal.

In this report we provide a summary of some of the "traditional" data analysis methods used for the calibration of underwater electroacoustic transducers, and indicate some of their limitations. We then give a brief introduction to wavelet analysis, and consider how methods of analysis based on wavelets can be applied to this particular measurement problem. The intention here is to consider how wavelet analysis may support and complement the "traditional" methods of analysis by addressing some of the limitations of those methods.

ISSN 1471–0005

National Physical Laboratory
Queens Road, Teddington, Middlesex, TW11 0LW



Approved on behalf of the Managing Director, NPL
by Dr D Rayner, Head, Centre for Mathematics and Scientific Computing

**TABLE OF CONTENTS**

# 1 INTRODUCTION

## 1.1 BACKGROUND

Electroacoustic transducers are used in underwater acoustics to generate and detect acoustic fields. If such devices are to make meaningful and quantitative measurements, the transducers must be calibrated and in a way that is traceable to national standards. The calibration method adopted at the National Physical Laboratory (NPL) is based on the principle of reciprocity [1], and depends on being able to measure the voltage generated by a transducer (acting as a receiver) placed in the acoustic field produced by another transducer (acting as a transmitter). In practice, however, the measurement is made difficult because the measured voltage is contaminated by a number of effects, including transients due to the resonances of the devices, reflections of the transmitted signal, and noise (Section 1.2).

Data processing is used to extract from the measured data the required information for the calibration, viz., the voltage that would be measured in a free-field environment and free from these contaminating effects. There are a number of approaches to performing the data analysis, including the application of signal processing techniques based on Fourier analysis as well as regression modelling, and each may require the measured signal to be “gated” to isolate a portion of the waveform to be analysed (Section 2).

Wavelet analysis provides another approach to analysing spectrally varying sequences of data that complements the traditional Fourier analysis. Wavelets provide a general set of basis functions that are localised both in time and frequency [2], and wavelet analysis has been applied successfully to problems in feature recognition [3, 4], signal compression [3], function representation [2] and as a basis for numerical schemes [5]. The coefficients obtained in a wavelet expansion are useful as they relate directly to a time (or place) and frequency, and to the smoothness of the signal.

The purpose of the report is twofold. Firstly, we provide in Section 2 a summary of some of the “traditional” data analysis methods indicated above, and discuss their limitations. The methods include those that operate on that part of the waveform corresponding to the echo-free time (before the arrival of reflections), and those that operate on measurements made in a reverberant field, i.e., where the measured waveforms are contaminated by reflections of the transmitted signal. The review is intended only to summarise the methods and not to be exhaustive: for more complete descriptions, see [6] and the references cited therein. Secondly, we give in Section 3 a brief introduction to wavelet analysis [7], and consider how methods of analysis based on wavelets can be applied to this particular calibration problem. The intention here is to consider how wavelet analysis may support and complement the “traditional” methods of analysis by addressing some of the limitations of those methods. Section 4 contains our conclusions, and indicates further work.

Throughout this report results have been produced using the MATLAB Technical Computing Environment [8] and functions provided in the MATLAB Signal Processing Toolbox [9] and MATLAB Wavelet Toolbox [10].

## 1.2 MEASUREMENT PROBLEM

A number of parameters may be used to describe the performance and characteristics of a transducer, including its *receive sensitivity* and *transmitting response*. The receive sensitivity $M_H$ of a hydrophone $H$ at a chosen frequency and in a stated direction is defined to be the quotient of the open-circuit voltage $V_H$ across $H$ and the acoustic pressure $p$ which would exist at the location of $H$ in the acoustic field if $H$ were removed:

$$M_H = \frac{V_H}{p}.$$

The transmitting response $S_P$ of a transmitter (projector) $P$ at a given frequency and in a given direction is defined as the quotient of the acoustic pressure $p$ at a reference distance from the acoustic centre of the projector and the current $I_P$ flowing through its terminals:

$$S_P = \frac{p}{I_P}.$$

There are a number of ways in which reciprocity-based calibration methods may be implemented [1], but they all involve the electrical measurement of the current driving a projector and the voltage generated by a hydrophone placed in the acoustic field produced by the projector. The method used at NPL involves three transducers and the above electrical measurements are made using pairs of the transducers. Assuming at least one of the devices is reciprocal, the transmitting or receiving sensitivity of any of the three transducers can be estimated from these purely electrical measurements. For example, if we use $P$ (projector), $H$ (hydrophone) and $T$ (reciprocal device) to denote the three devices, the receive sensitivity of $H$ is given by

$$M_H = \sqrt{J \frac{d_{PH} d_{TH}}{d_{PT}} \frac{Z_{PH} Z_{TH}}{Z_{PT}}}, \tag{1}$$

where, for example, $d_{PH}$ is the separation distance from $P$ to $H$, and $Z_{PH}$ is the transfer impedance when transmitting with $P$ and receiving with $H$, i.e.,

$$Z_{PH} = \frac{V_H}{I_P},$$

with $V_H$ denoting the voltage across $H$ and $I_P$ the current applied to $P$. For a spherical-wave field, the reciprocity parameter $J$ is given by $J = 2/\rho f$ where $\rho$ is the water density and $f$ is the acoustic frequency.

Having calibrated a reference hydrophone in this way, it can then be used to obtain information about another un-calibrated projector. For example, the transmitting voltage response $S_P$ of the projector may be written as

$$S_P = \frac{V_H d_{PH}}{V_P M_H}, \tag{2}$$

with $V_P$ denoting the voltage applied to $P$, $V_H$ the voltage across $H$ when placed in the acoustic field produced by $P$, and $M_H$ given by (1).

The free-field calibration of underwater electroacoustic transducers described above requires a free-field environment in which there is no interference caused by boundary reflections. For continuous wave fields, this requirement implies the use of a large volume of water such as a lake, reservoir or ocean in order that reflections from the medium boundaries are sufficiently attenuated by propagation losses. The impracticality and expense of utilising such volumes has led to the use of laboratory tanks for making measurements with time-windowing and the application of signal processing techniques to extract free-field information from the measurements. Laboratory tanks have the advantage of providing more controlled experimental conditions, but their use introduces measurement problems, especially if the tank dimensions are small when measured in acoustic wavelengths.

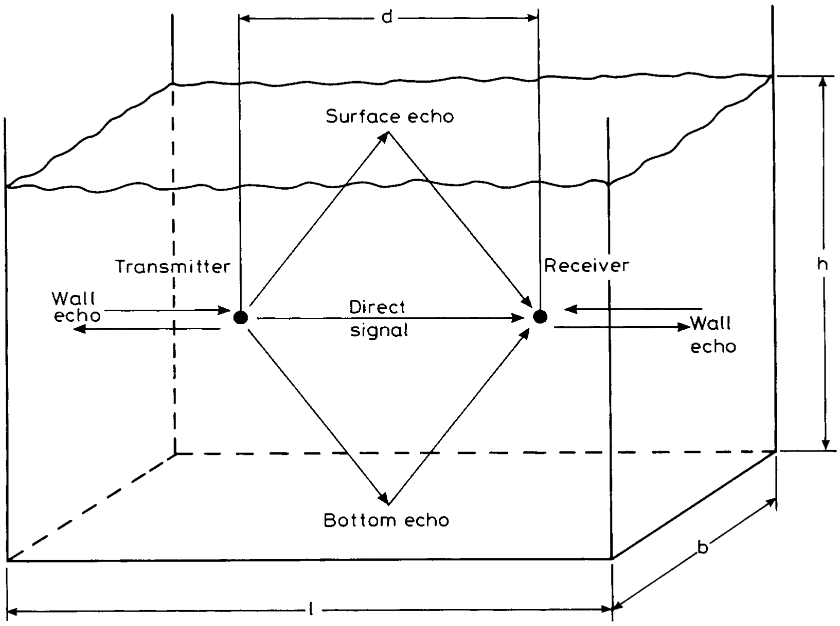


**Figure 1:** Schematic diagram of a transmitter (projector) and receiver in a water tank showing the main sources of reflections (ignoring multiple reflections).

In this work we are concerned with the measurement arrangement illustrated in Figure 1 in which two transducers, one acting as a transmitter (projector) and the other as a receiver, are suspended in a tank of finite size filled with water. The projector is driven by a *tone-burst*, i.e., a sinusoidal signal of single frequency and finite duration, and it is required to determine from measurements of the voltage across the receiving hydrophone the (steady-state) voltage $V_H$. This information is then used in the calibration formulae (1) and (2).

However, the signal detected by the receiving hydrophone is contaminated by:

- transients due to the resonances of the devices,
- reflections of the transmitted signal from the tank walls, floor and the water-surface, and
- noise (potentially from both acoustic and electrical sources).

The extra distance travelled by the reflected signals causes them to arrive later in time than the direct path signal. The time available to observe the direct signal before the reflections arrive is termed the *echo-free time*, and depends on the size of the tank and the locations of the transducers within it. Figure 1 shows the direct signal path and the main sources of reflections (ignoring multiple reflections).

The received signal is sampled at uniformly spaced times by use of an analogue-to-digital converter. Figures 2 and 3 show some waveforms obtained in this way for a projector with a resonance frequency of approximately 18 kHz and a receiver with no resonance frequency close to any of the tone-burst frequencies.[1] The projector is driven by a sequence of tone-

[1] This choice of a receiver with no resonance frequency close to the tone-burst frequencies ensures that

bursts of frequencies 5 kHz to 25 kHz in steps of 1 kHz and each of a specified duration. Waveforms corresponding to frequencies of 5 kHz, 18 kHz and 25 kHz, that are respectively below, close to and above the resonance frequency of the projector, are shown in the figures. To obtain the waveforms shown in Figure 2 the transducers are placed close to the centre of the tank, and for those shown in Figure 3 the transducers have been raised in the tank to be close to the water surface. For each waveform the (approximate) echo-free time window is indicated by vertical dotted lines: when the transducers are placed close to the centre of the tank, the echo-free time is set (conservatively) to be about 350 μs, whereas for the waveforms shown in Figure 3 it lasts for about 35 μs, i.e., for approximately two-thirds of a cycle of the resonance frequency of the projector.

We can identify in the waveforms of Figure 2 the various "stages" in the responses as follows. The waveform starts when the projector is turned on (corresponding to the start of the tone-burst), followed immediately by an oscillation at its resonance frequency. Once the resonant behaviour is sufficiently damped, we observe the steady-state response of the device in the form of an undamped oscillation at the frequency of the tone-burst. Finally, the response is contaminated by a combination of the device being turned off and the arrival of the first reflections. The required measurement result $V_H$ is the amplitude of the steady-state component of this response.

For the waveforms shown in Figure 2, direct measurement of the steady-state amplitude is possible.[2] However, in cases where the echo-free time, the tone-burst frequency and the $Q$-factor for the device (which measures the "damping" of the device) combine so that the steady-state response cannot be observed, it is necessary to apply data analysis and signal processing techniques to estimate the steady-state amplitude $V_H$. Such cases are illustrated in Figure 3, and are the subject of this report.

## 2 TRADITIONAL METHODS OF ANALYSIS

### 2.1 FOURIER ANALYSIS

The standard Fourier transform (FT)

$$Y(\omega) = \int y(t)e^{-i\omega t}dt$$

of a signal $y(t)$, where $\omega = 2\pi f$ is the angular frequency, provides a representation of the frequency content of $y$. It describes the decomposition of $y$ into sinusoidal components of different frequencies by providing information about the amplitude and phase of these components. Because the decomposition is in terms of components that are not localised, a drawback of the Fourier transform is that information concerning time-localisation is lost. Such information is important, for example, for non-stationary signals of the type considered here for which the frequency content of the signals changes with time.

the observed waveform is contaminated by transients due to the resonance of the projector *only* and not those of the receiver.

[2] For the projector considered here and the particular measurement arrangement considered, 5 kHz is probably the lowest tone-burst frequency for which direct measurement of the steady-state amplitude is possible. For the waveform corresponding to this frequency there appears to be about 1 cycle of the steady-state response available for analysis.

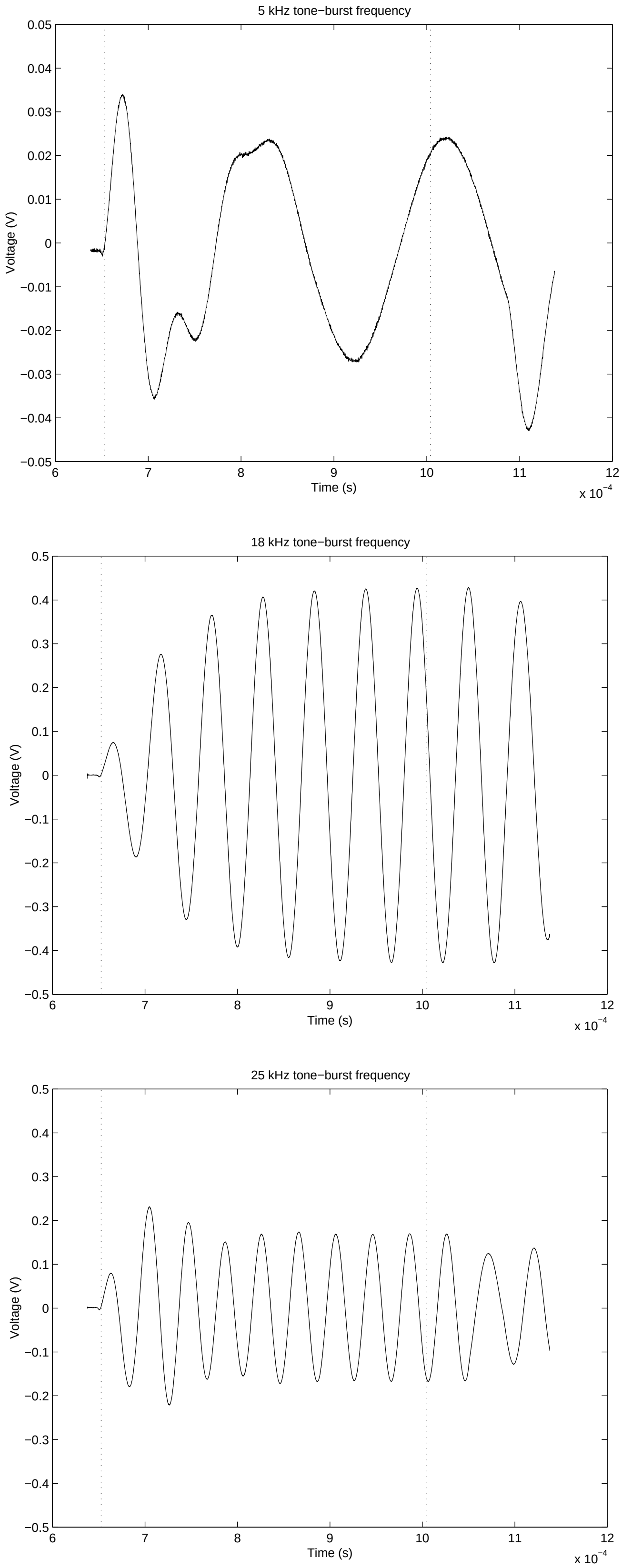


**Figure 2:** Measured voltage waveforms for a given projector and receiver corresponding to drive frequencies of (a) 5 kHz, (b) 18 kHz and (c) 25 kHz. A time window of approximately 350 μs containing the steady-state response is indicated.

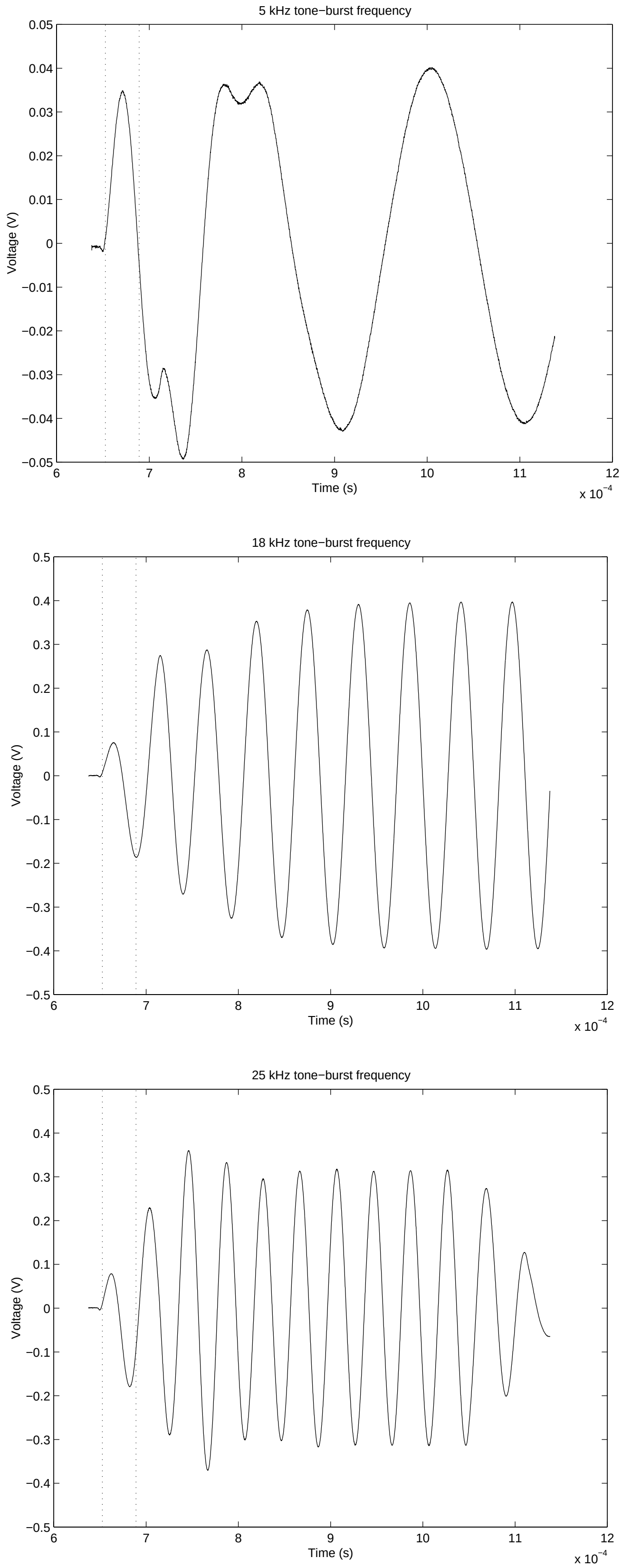


**Figure 3:** Measured voltage waveforms corresponding to those in Figure 2, viz., for 5 kHz, 18 kHz and 25 kHz drive frequencies, but in the presence of a reflection at (approximately) 65 μs after the arrival of the direct signal. The echo-free time of approximately 35 μs is indicated.

Some localisation in time can be achieved by first windowing the signal $y$, so as to define localised portions of the signal, and then applying the Fourier transform to each portion:

$$Y^{win}(t,\omega) = \int \{y(s)g(s-t)\}e^{-i\omega s}\,ds,$$

where $g$ is a windowing function. This scheme, known as the short-time Fourier transform (STFT), gives some information about both when and at which frequencies an event occurs, but the accuracy with which such information is determined is dependent on the size of the window and the nature of the windowing function. Furthermore, it is not possible to achieve high accuracy in both time and frequency. To obtain high accuracy in one variable it is necessary to compromise accuracy in the other.

The *spectrogram* provides a tool for visualising the STFT of a signal. It is a graph of the amplitude of the STFT, computed using the Fast Fourier Transform (FFT)[3] [11], and plotted against time and frequency. The spectrogram provides information about how the Fourier transform, and hence the frequency content, of a signal changes with time. The spectrograms for the signals shown in Figures 2 and 3 are shown in, respectively, Figures 4 and 5.[4]

It is difficult to identify in these graphs features of the original signals, or to use the results to provide quantitative information about the signal and its components. In Section 3.1 we consider an analysis of the signals using the continuous wavelet transform (CWT) that also provides a time-frequency decomposition of the signal. The CWT decomposes the signal into components (wavelets) that are locally defined giving somewhat easier interpretation of the results. Some discussion comparing the STFT and CWT is given in [2].

## 2.2 ANALYSIS OF FREE-FIELD SIGNAL

In the case of the signals shown in Figure 2, there is sufficient time before the arrival of the first echoes for the steady-state signal to be observed directly. Typically, a time-window or gate is applied so that only the portion of the steady-state signal within the window is made available for analysis. There are a number of ways in common usage for measuring the amplitude of the steady-state component. These include:

(i) Measurement of the peak voltage, directly by a peak detector or by measuring the maximum and minimum of the digitised signal.
(ii) Calculating the root-mean-square (RMS) voltage. Ideally, to avoid bias in the result, an integer number of cycles of the sinusoidal signal is used.
(iii) Performing a Fast Fourier Transform (FFT) of the signal and taking the amplitude of the spectrum at the drive frequency, again using an integer number of cycles.
(iv) Performing a "narrow-band" discrete Fourier transform (DFT) of the signal, calculating only the amplitude of the component at the drive frequency, again using an integer number of cycles.
(v) Performing a least-squares fit of the signal by a sine-wave of the appropriate frequency and taking the amplitude of the fitted sine-curve.

---

[3] In practice, the signal $y$ is *sampled*, i.e., it is known only in terms of its values $\{y_k\}$ at equally spaced points in time. The *discrete Fourier transform* (DFT), calculated in terms of the values $\{y_k\}$, provides an estimate of the Fourier transform. The *Fast Fourier Transform* (FFT) is a fast algorithm for computing the DFT.
[4] In these graphs, time is measured from the start of the signal (cf. Figures 2 and 3).

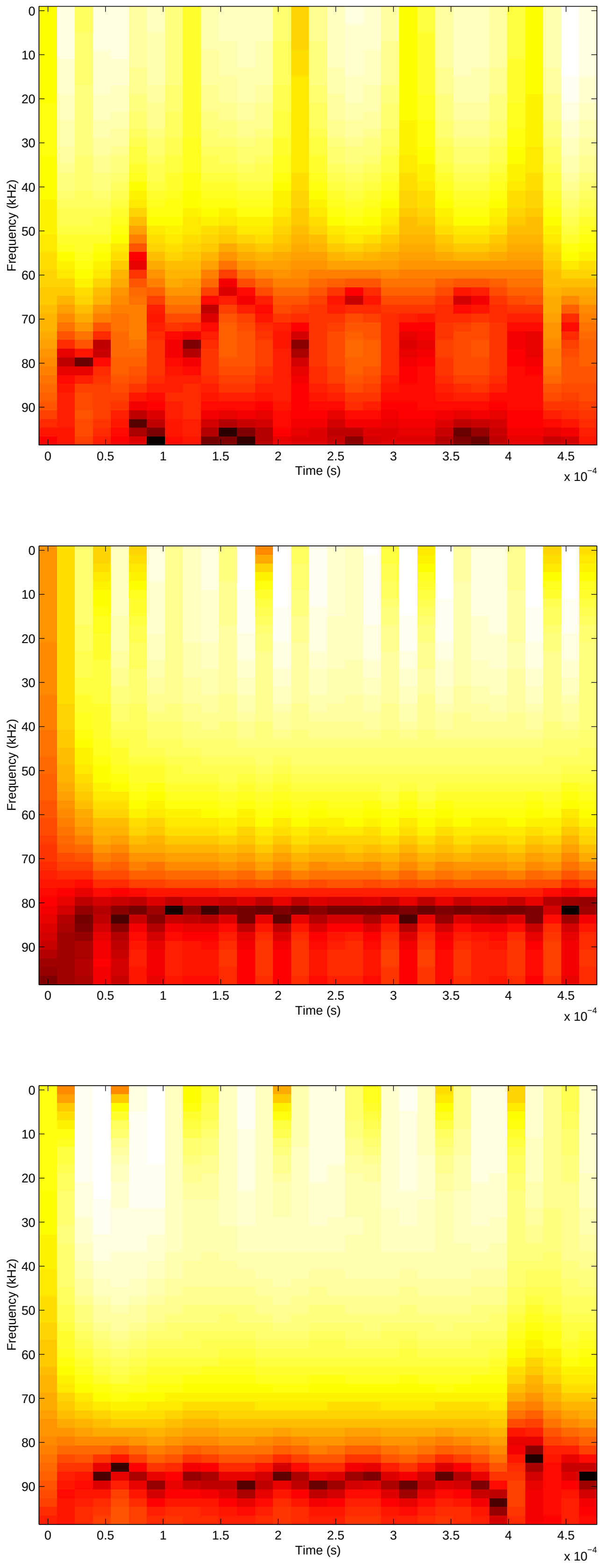


**Figure 4:** Spectrogram (windowed Fourier transform) of the signals shown in Figure 2: (a) 5 kHz, (b) 18 kHz, and (c) 25 kHz drive frequencies.

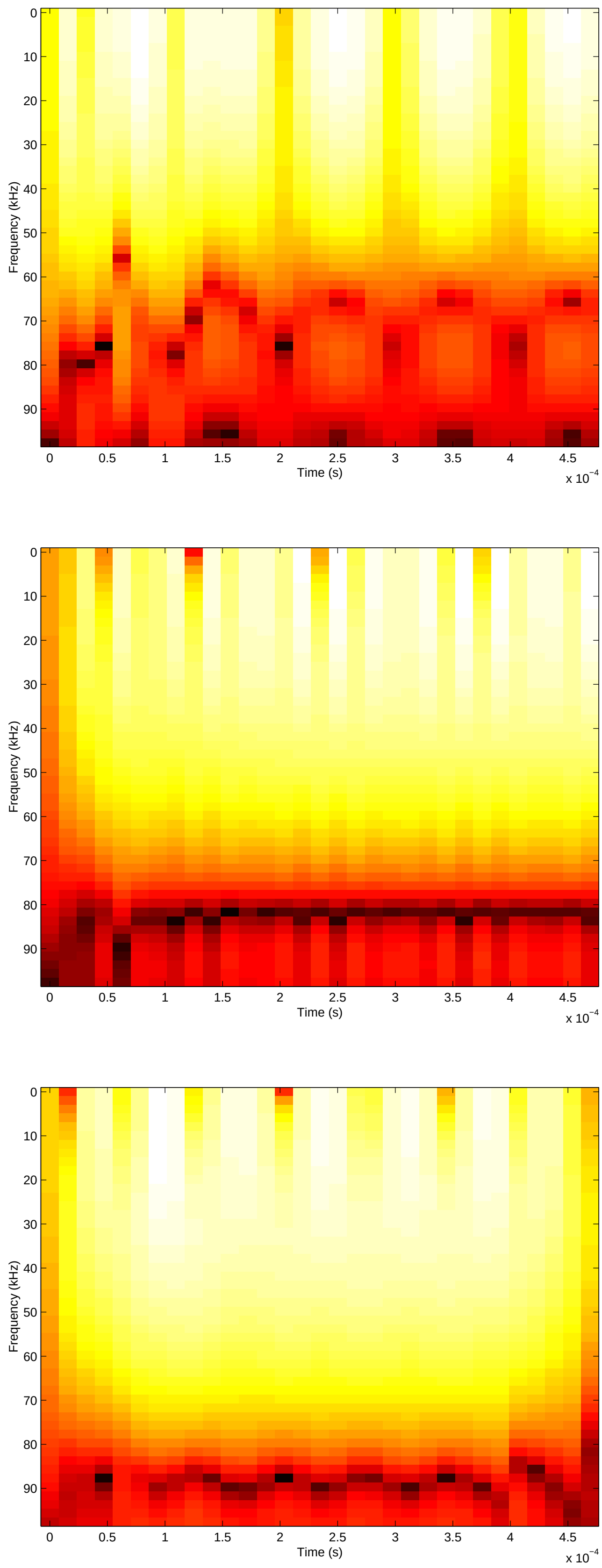


**Figure 5:** Spectrogram (windowed Fourier transform) of the signals shown in Figure 3: (a) 5 kHz, (b) 18 kHz, and (c) 25 kHz drive frequencies.

All the above methods have strengths and weaknesses. The peak measurement of (i) is simple to implement but inaccurate in the presence of any noise, distortion and residual amplitude fluctuations of the waveform envelope. The other methods all require more processing, perhaps with dedicated software algorithms. However, methods (ii) to (v) will effectively provide some averaging of small amplitude variations if many cycles are contained within the time window. Methods (iii) to (v) will also provide some discrimination against noise and information on phase as well as amplitude. However, bias will arise with methods (ii) to (iv) if an integer number cycles is not used for the analysis. A further issue with the FFT of method (iii) is that the spectrum might not contain a point at the exact frequency of excitation. Depending on the number of cycles available for analysis, methods (ii), (iv) and (v) are generally used at NPL. Both methods (iv) and (v) can still be useful even when analysing only half a cycle of signal.

As we have already noted, in the examples from Figure 2 the steady-state signal can be observed directly and the methods indicated can be expected to give useful estimates. However, fewer cycles of the steady-state signal are available for analysis at lower frequencies since the period increases with decreasing frequency. If the echo-free time for a particular tank with transducers optimally positioned is denoted by $T$, the number of cycles available for analysis before the arrival of reflections is equal to the product $fT$, where $f$ is the frequency of excitation. If these cycles are to be used for analysis, steady-state conditions must be reached if one of the above methods is to be employed. Since the electroacoustic transducers used in underwater acoustics are resonant devices behaving as damped harmonic oscillators of quality-factor $Q$, it will take approximately $Q$ cycles of the resonance frequency before the initial transients have decayed. For situations where $Q > fT$, so that steady-state is not reached within the free-time available, *all* the methods described above will lead to inaccurate values for the steady-state amplitude. Such situations are illustrated in Figure 3.

## 2.3 SIGNAL MODELLING

For the conventional methods of Section 2.2 it is necessary for the echo-free time to be sufficiently long and the device adequately damped for the steady-state response to be observed directly. In this section we present methods based on *signal modelling* that allow these requirements to be relaxed by extending the part of the signal that is analysed. In Section 2.3.1 the part of the signal analysed is extended to include the initial transient-dominated part of the waveform. Nevertheless, as illustrated using the waveforms shown in Figure 3, this approach may still involve discarding a large amount of data, and hence information. Therefore, in Section 2.3.2 we further extend the part of the signal analysed to include reflections.

### *2.3.1 Analysis of data measured in the echo-free time*

The difficulties outlined in Section 2.2 may be overcome to some degree if greater use can be made of the initial transient-dominated part of the waveform. If we consider the response of an electroacoustic transducer at frequencies at or below its first resonance frequency, it is reasonable to assume the behaviour to be that of a damped harmonic oscillator. This behaviour corresponds to the regime where the device may be modelled with a so-called "lumped-parameter" model. The behaviour of a damped harmonic oscillator is governed by a linear constant-coefficient differential equation of the kind familiar from the analysis of systems of masses, springs and dampers (or, in an electrical analogue, a resonant LCR circuit). The solutions of such a differential equation are also well known, and may be expressed as combinations of undamped and damped sinusoids, e.g.,

$$V(t) = A_0 \sin(2\pi f_0 t + \phi_0) + \sum_{k=1}^{n_r} A_k e^{-d_k t} \sin(2\pi f_k t + \phi_k), \tag{3}$$

where the first term represents the steady-state component of the response to the drive signal (and has a frequency $f_0$ equal to that of the drive signal) and the summation represents the resonant behaviour of the device. Alternatively, the voltage response may be written as a sum of (complex) exponentials

$$V(t) = \sum_j \alpha_j e^{\beta_j t}, \tag{4}$$

where the $\alpha_j$ and $\beta_j$ are, respectively, complex-valued residues and poles. Such functions may be used to model the signal observed from the start of the tone-burst until the first reflection arrives [12, 13].

A data approximation problem is posed in which estimates of the parameters defining the model (3) or (4) are obtained to best-fit the measured data values in a least-squares sense, i.e, given data $\{(t_i, v_i): i = 1, \ldots, m\}$, the estimation problem

$$\min \quad \sum_{i=1}^{m} \left(v_i - V(t_i)\right)^2$$

is solved. Since the signal model is non-linear (it is composed of exponential functions with unknown time constants), the estimation problem is solved using a nonlinear least-squares algorithm such as the Gauss-Newton algorithm. Other estimators have also been proposed, such as linear prediction estimators that include the classic method of Prony.

The technique allows measurements to be made on transducers at frequencies lower than that at which the techniques of Section 2.2 may be successfully used. In addition to providing information on the steady state amplitude, the model includes parameters relating to phase, and the phase response of the transducer may also be extracted. The results presented in [12, 13] indicate that for moderately resonant transducers, errors of less than 1 dB in the estimate of the transmitting voltage response $S_P$ will result if data representing approximately one cycle of the resonance frequency is available for the analysis.

However, in cases where less than one cycle of resonance is available, this level of accuracy is difficult to achieve using the approach described. Consider the measurements described in Section 1, and illustrated by the waveforms shown in Figures 2 and 3. As we have previously noted, when the devices are located close to the centre of the tank (and we obtain waveforms as illustrated in Figure 2) the steady-state response of the projector may be observed. Consequently, it is possible to make a direct measurement of the (free-field) steady-state amplitude $V_H$ from which the (free-field) transmitting voltage response $S_P$ may be obtained using (2).[5] For each waveform, we fit the data contained within the echo-free time (indicated in Figure 2) by a model composed of an undamped sinusoid with a frequency given by that of the corresponding tone-burst and a single ($n_r = 1$) damped sinusoid to represent the resonant behaviour, and estimate $V_H$ from the fitted model.

The same data processing procedure is then applied to the measurements obtained when the devices are moved towards the water surface (and we obtain waveforms as illustrated in Figure 3). However, the procedure is applied using data contained within a time-window

[5] We assume that the distance $d_{PH}$ between the transducers, the amplitude $V_P$ of the tone-burst, and the sensitivity $M_H$ of the receiver (a calibrated device) are known or measured.

defining the echo-free time (indicated in Figure 3) that lasts only for approximately two-thirds of the device's resonance period.

The estimates of the transmitting voltage response $S_P$ obtained from the two sets of measurements are shown in Figure 6, and the differences between the estimates are presented in Figure 7. We see that the difference is of the order of 3 dB close to the resonance frequency, and as much as 5 dB for the lowest frequencies considered. The achieved accuracy is insufficient for the primary calibrations undertaken by NPL.

### *2.3.2 Analysis of data measured in the reverberant field*

To apply the signal modelling techniques described in Section 2.3.1 to data within a time-window extended to include the first few reflections we augment the model (3) to include *delayed* terms to represent the arrival of reflections as follows. We write the signal model in the form

$$V(t) = \sum_{i=0}^{N} V_i(t, \tau_i) H(t - \tau_i), \tag{5}$$

where

$$H(t) = \begin{cases} 0, & t < 0, \\ 1, & t \geq 0, \end{cases}$$

is the unit step function,

$$V_i(t, \tau_i) = A_{0,i} \sin\big(2\pi f_0 (t - \tau_i) + \phi_{0,i}\big) + \sum_{k=1}^{n_r} A_{k,i} e^{-d_k (t - \tau_i)} \sin\big(2\pi f_k (t - \tau_i) + \phi_{k,i}\big), \tag{6}$$

and $\tau_i$, $i$ = 1, …, $N$, are the echo arrival times with $\tau_0$ defining the start of the tone-burst. Notice that in the model (6) for each reflection, some parameters, viz., the steady-state and resonance frequencies and the damping factors, are common because they are determined by the drive signal (tone-burst) and properties of the device, whereas the amplitudes and phases of the components vary from reflection to reflection. The required steady-state amplitude $V_H$ is denoted here by $A_{0,0}$, i.e., it is the amplitude of the undamped sinusoid component of $V_0(t, \tau_0)$, the response to the direct signal.

Estimates of the model parameters are obtained by finding the least-squares fit by the function of the form (5) to the measured data. If accurate estimates of the echo arrival times $\tau_i$, $i > 0$, are known or can be determined, this process reduces to a nonlinear least-squares problem that is very similar to that arising in Section 2.3.1. If estimates of the echo arrival times are not known, they are determined as part of the fitting process.

This approach, in which a multipath model is fitted to measured data, has been considered in [14, 15]. To see the results that can be obtained we return to the measurements described in Section 1, and illustrated by the waveforms shown in Figures 2 and 3. As before, we apply the signal modelling techniques of Section 2.3.1 to the measurements made with the devices close to the centre of the tank to obtain an estimate of the (free-field) transmitting voltage response $S_P$. However, to analyse the measurements made with the devices close to the water surface (for which the waveforms shown in Figure 3 are examples) we model the data contained within a time-window (of length approximately 350 μs) that includes the first reflection with a function of the form (5) with $N = 1$ and $n_r = 1$.

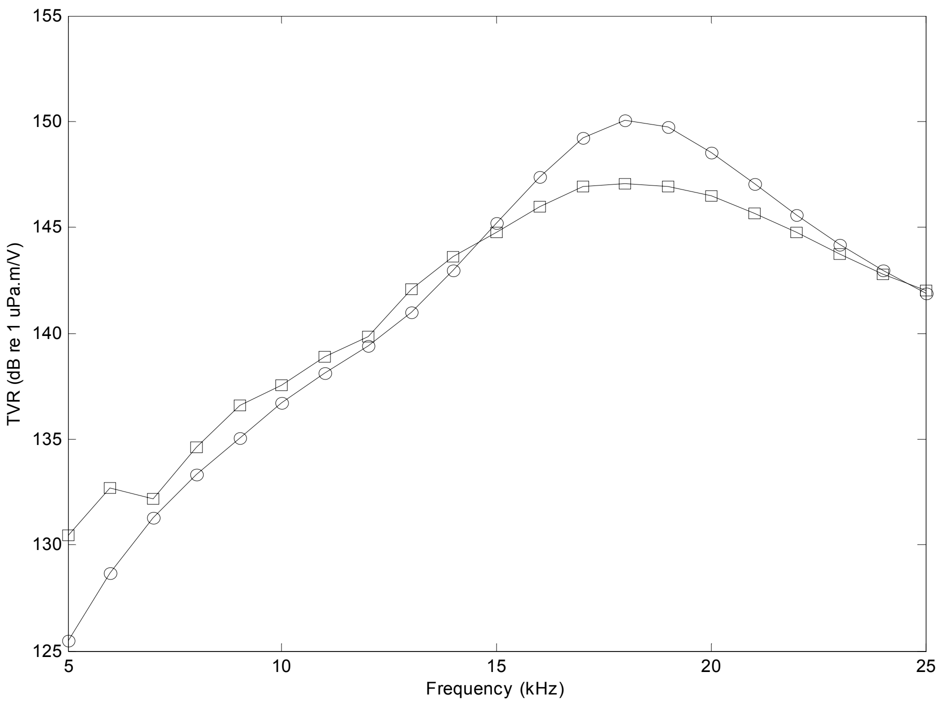


**Figure 6**: Transmitting voltage responses $S_P$ obtained from (i) free-field measurements (circles), and (ii) measurements made during an echo-free time of approximately two-thirds of a cycle of the device's resonance (squares).

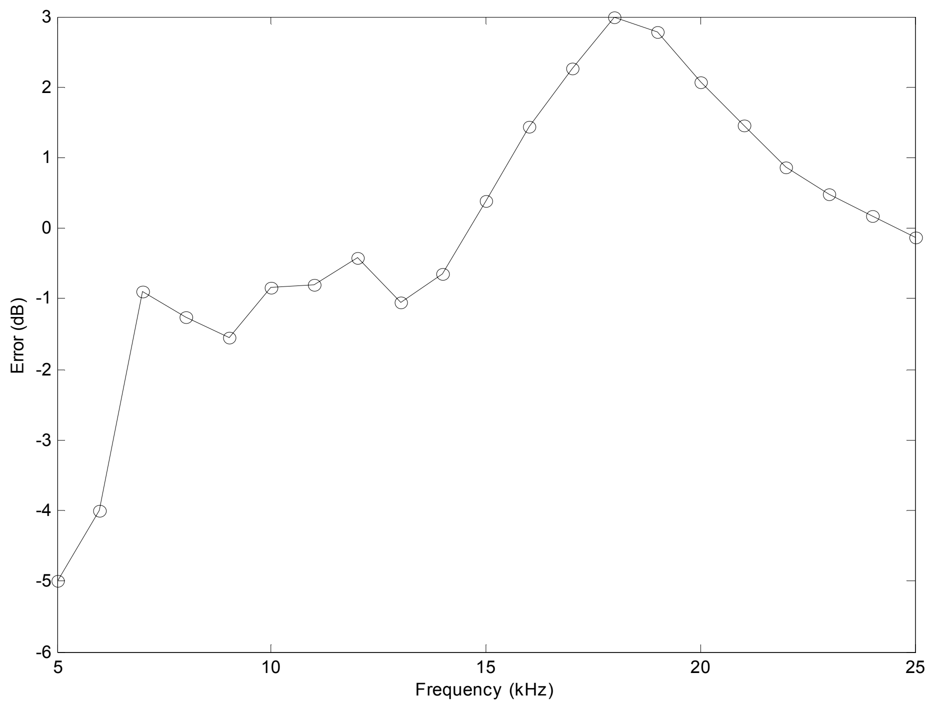


**Figure 7**: Differences between the transmitting voltage responses shown in Figure 6.

The estimates of the transmitting voltage response $S_P$ obtained from the two sets of measurements are shown in Figure 8, and the differences between the estimates are presented in Figure 9. We see that an accuracy of 1 dB is achieved across (almost) the complete frequency range and, consequently, there is an improvement over the results given in Figures 6 and 7 obtained using the simpler signal model. However, for any given size of tank there will be a frequency (depending on the transducer *Q*-factor) where the accurate use of signal modelling techniques becomes impossible.

Our experience of analysing real data using the signal modelling techniques described leads to the following observations:

a) The success of these techniques is to a large extent dependent on the amount of noise present in the data. In particular, linear prediction estimators, including the classical method of Prony, that are used to provide initial estimates for the (Gauss-Newton) algorithm used to solve the non-linear least-squares estimation problem, are notoriously sensitive to the presence of noise [12].

b) The methods tend to perform better when the arrival times are treated as (known) fixed parameters rather than as free parameters to be determined as part of the optimisation [13].

These observations suggest the potential application of wavelet analysis for de-noising (Section 3.2) and feature identification (Section 3.3).

## 2.4 FILTERING TECHNIQUES

The techniques presented in Sections 2.2 and 2.3 involve applying operations to the data, such as *fitting* and *smoothing*, within the domain of the data: this is the time domain for the measured waveforms, examples of which are shown in Figures 2 and 3.

The approaches described in this section use *filtering* to remove the effects of reflections. They are based on:

1. making measurements in a reverberant field,

2. applying a transformation to the measurements,

3. modifying the measurements in the transformed domain to remove unwanted features, e.g., by applying a suitable window function, and finally

4. transforming the modified measurements back to the original domain.

The techniques include filtering the transmitting voltage response using Fourier analysis and cepstral analysis (Section 2.4.2). Wavelet analysis, particularly based on the discrete wavelet transform (DWT), provides another transformation of the data that can potentially be used as the basis of filtering in the manner described above. Such analysis is described in Section 3.

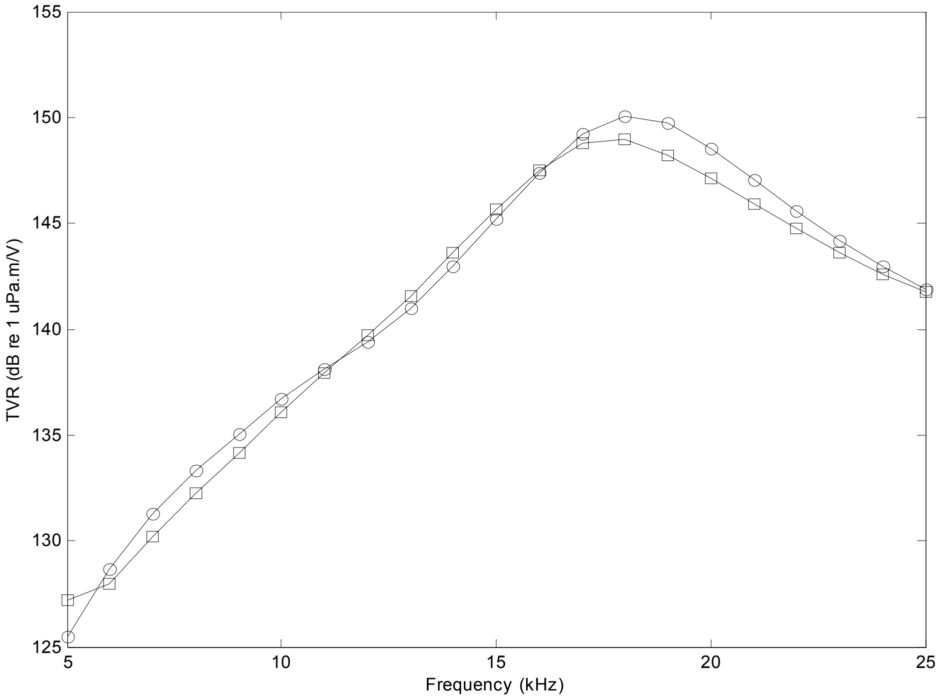


**Figure 8**: Transmitting voltage responses $S_P$ obtained from (i) free-field measurements (circles), and (ii) measurements made during an extended time-window that includes a single reflection (squares).

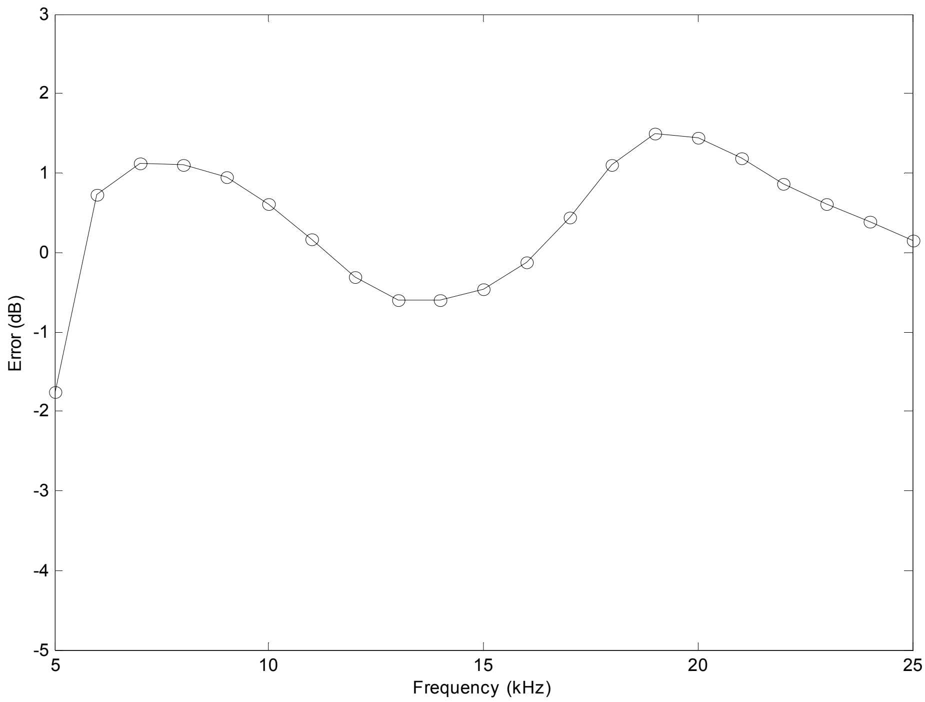


**Figure 9**: Differences between the transmitting voltage responses shown in Figure 8.

### *2.4.1 Fourier analysis*

The results of transducer calibration in a reverberant field show the influence of acoustic reflections, which manifest themselves as perturbations of the true free-field frequency response of the transducer under test. An example of these results is given in Figure 10 where the free-field transmitting voltage response $S_P$ of a projector is compared with that obtained from measurements made at discrete frequencies in a reverberant tank.

In this technique the Fourier transform is applied to the measured transmitting voltage response illustrated in Figure 10 to give the signal shown in Figure 11(a). In the latter figure, the presence of a reflection after about 1.5 ms is clearly visible. The transformed signal is modified by applying an appropriate windowing function to remove that part of the signal representing the reflection. The inverse Fourier transform is then applied to the modified signal to give an estimate of the transmitting voltage response that is free of the reflection. Figure 11(b) shows the original measured response (in black), the estimate of the response constructed in this way (in blue), and for comparison the free-field response (in red).

In this illustration of the method, a simple rectangular window is used to filter the signal, and this choice is responsible for some of the perturbations in the estimated response, particularly at the ends of the frequency range.

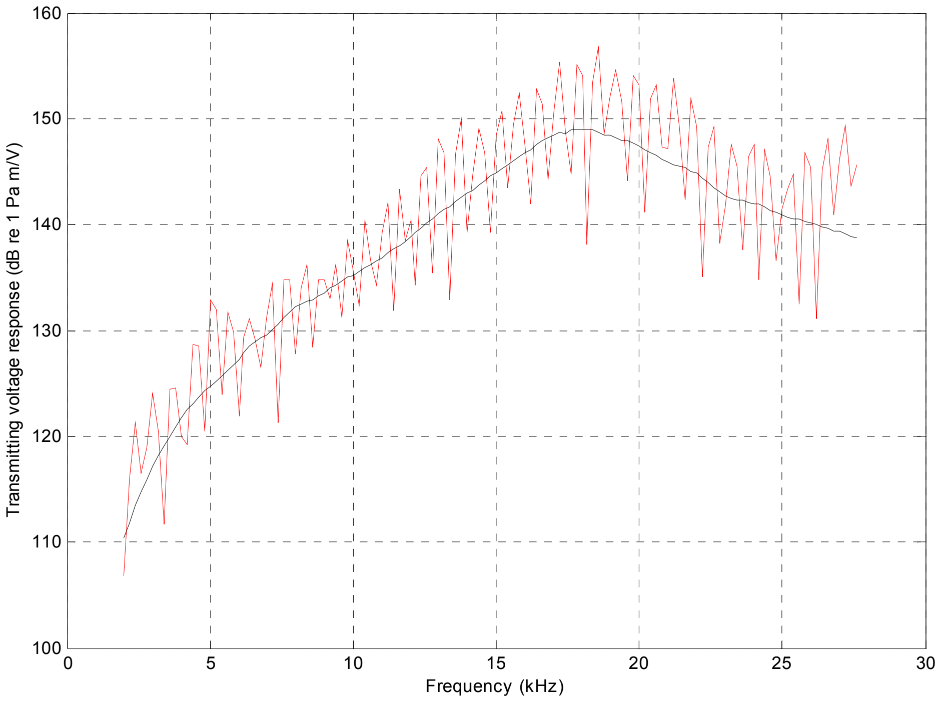


**Figure 10**: Transmitting voltage response $S_P$ of a projector measured in a reverberant tank showing the influence of reflections. For comparison, the free-field transmitting voltage response is shown as a smooth curve.

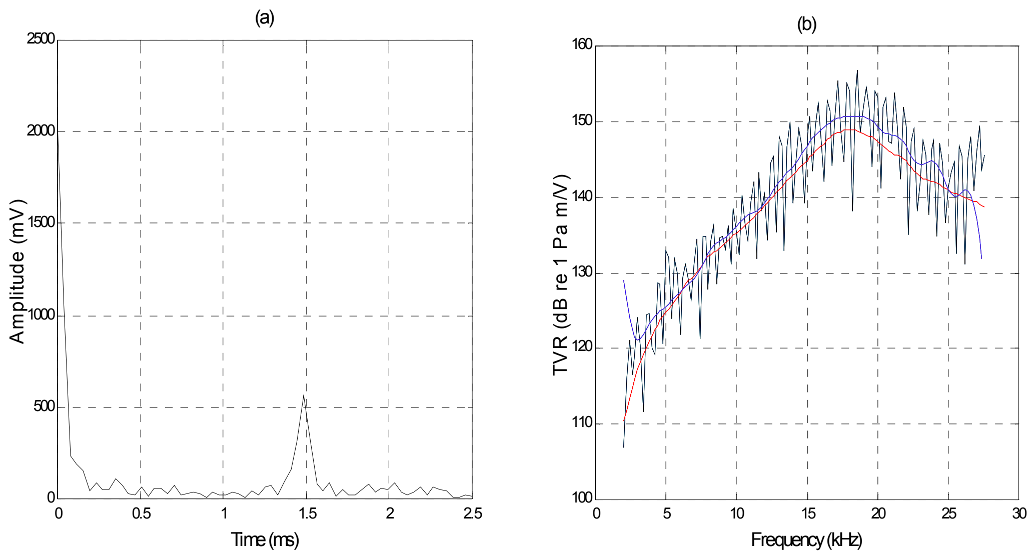


**Figure 11**: Results of smoothing in the time-domain: (a) the time-domain data before windowing; (b) comparison of the original data (black), free-field response (red), and smoothed response (blue).

### *2.4.2 Cepstral analysis*

The complex cepstrum C(τ) of a time-domain signal $y(t)$ is defined by

$$C(\tau) = \Im^{-1}\{\ln(\Im\{y(t)\}\},$$

where "ln" is the complex natural logarithm and $\Im$ is the Fourier transform operator.

The cepstrum of a signal has the following useful properties. Firstly, those parts of the spectrum that vary slowly (and are typical of smooth transfer functions) tend to be gathered around the origin in the cepstral domain, whereas rapid spectral variations (for example those caused by the arrival of reflections) are not moved. Secondly, because of the logarithm operation, signals that are convolved in the time domain $t$, and hence multiplied in the spectral domain $f$, are summed in the cepstral domain τ. These properties enable convolved effects in time signals to be identified in the cepstral domain and removed by subtraction before applying the inverse cepstrum transformation.

Figure 12 illustrates the application of cepstral analysis, or homomorphic signal processing as it is sometimes called, to the elimination of reflections from a time signal. The free-field signal illustrated in Figure 12(a) is contaminated with reflections as shown in Figure 12(b). The complex cepstrum of the signal containing reflections is shown in Figure 12(c) in which the positions of rapid spectral variation corresponding to the arrival of reflections are clearly visible. Figure 12(d) is a modified version of the cepstrum that is used to reconstruct the signal shown in Figure 12(e). Figure 12(f) shows the residual differences between the reconstructed signal and the original free-field signal.

The free-field signal used in the example of Figure 10 might simulate the response of a resonant device to a pulse signal. With other signals it can be difficult to subtract the contributions of reflections without prior knowledge. However, if the signal is broadband, the cepstrum shows a narrow peak and identification and removal of reflections is possible [16].

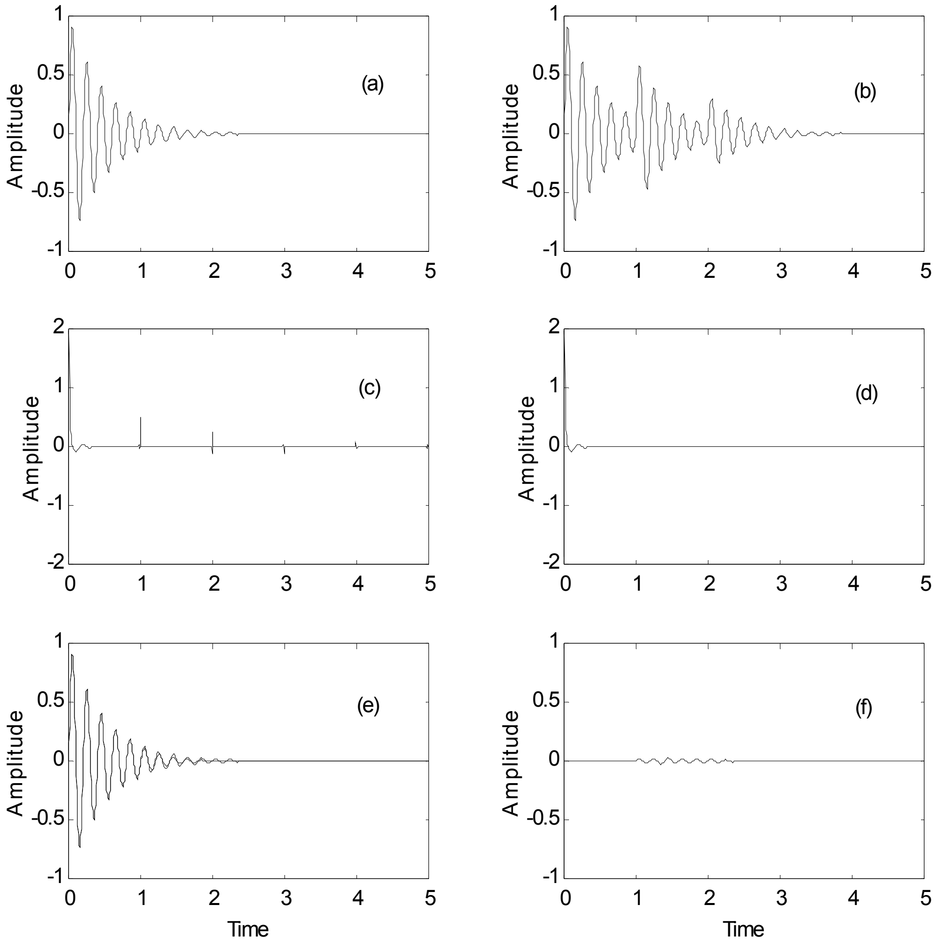


**Figure 12**: Illustration of removal of reflections using the complex cepstrum: (a) source signal; (b) source signal with two reflections; (c) complex cepstrum of signal with reflections; (d) filtered cepstrum; (e) reconstructed signal without reflections; (f) residual differences between reconstruction and original.

# 3 METHODS BASED ON WAVELET ANALYSIS

In Section 2 we have described a number of "traditional" data analysis and signal processing techniques for analysing data arising from the calibration of underwater acoustic transducers undertaken in reverberant laboratory tanks. In this section we consider how new methods based on wavelet analysis may be applied in this calibration problem.

## 3.1 WAVELET ANALYSIS

Wavelets may be thought of as oscillations that are localized in time (or space) and frequency. The representation of a function or signal in terms of wavelets is attractive because the coefficients defining that representation convey details in time and frequency. A small coefficient means there is little variation in the function or signal in the vicinity of that particular small oscillation, whereas a large coefficient indicates that there is appreciable change in the signal or function. Analysis of the coefficients allows features in the function or signal to be identified. Furthermore, because coefficients are identified with both a localized frequency and time, coefficients that are sufficiently small in absolute value can be replaced by zero without greatly affecting the reconstruction of the signal. This strategy leads to the efficient representation of functions and the de-noising of signals.

The combination of these localisation properties makes wavelets attractive for the following general signal processing problems:

1. de-noising (and smoothing) of signals,

2. detection of features in signals, and

3. sparse representation of functions.

For the acoustic application considered here we are more concerned with 1 and 2 as we wish to extract information from a measured waveform rather than simply determine an economic representation of the waveform.

Since wavelets offer a time-frequency decomposition, a common way to visualise the wavelet coefficients in a wavelet transform is in a time-frequency plot (where frequency relates to the wavelets rather than the traditional Fourier frequency). This plot is the equivalent of the spectrograms of Figures 4 and 5 from the (short) windowed Fourier transform. There are in fact a number of different forms of wavelet decomposition that can be applied. We shall consider the two most frequently applied: the continuous and discrete wavelet transforms. There follows a brief summary of these two transforms; a full description, along with a more complete review of wavelet techniques in the context of metrology, can be found in [7].

### *3.1.1 Continuous wavelet transform*

The continuous wavelet transform (CWT) is analogous to the standard Fourier transform, and gives a time-frequency decomposition by taking translations and dilations of a mother wavelet $\psi(t)$,

$$\Psi_{a,b}(t) = \frac{1}{\sqrt{|a|}} \psi\left(\frac{t-b}{a}\right),$$

where $a\,(\neq 0)$ and $b$ are real-valued, and $\psi(t)$ may be real- or complex-valued. The parameters $a$ and $b$ are referred to as the *scale* and *translation* parameters, respectively. The scale parameter controls the compressing or stretching of the mother wavelet: small values of $|a|$ produce a compressed wavelet, corresponding to high frequency or *detail*, whilst large values of $|a|$, producing a stretched wavelet, correspond to low frequency. The translation parameter controls the location of the wavelet in time.

The CWT of a function $f(t)$ (which we assume to be continuous) is given by

$$C(a,b) = \int f(t)\ \overline{\Psi_{a,b}(t)}\ \mathrm{d}t\ , \tag{7}$$

where $\overline{\Psi_{a,b}}$ denotes the complex conjugate of $\Psi_{a,b}$.

A signal can be reconstructed from its CWT by evaluating

$$f(t) = \kappa^{-1} \iint a^{-2} C(a,b) \frac{1}{\sqrt{|a|}} \psi\left(\frac{t\text{ - }b}{a}\right) \mathrm{d}a\ \mathrm{d}b, \tag{8}$$

where the constant $\kappa$ ($< \infty$) depends on the choice of mother wavelet $\psi$.

Note that for the CWT the parameters *a* and *b* are *continuous* variables. In practice, we generally deal with discrete forms of signals, in which case the parameters are typically bounded. Furthermore, for computational purposes, *a* and *b* are restricted to take discrete values.

The CWT can be visualised by plotting $C(a, b)$ against *a* and *b*. Figures 13 and 14 show CWTs for the waveforms shown in Figures 2 and 3 respectively. The transform is based on the choice of the Morlet wavelet [10] as the mother wavelet. In these plots, the vertical axis corresponds to the scale parameter *a*, the horizontal axis to the translation parameter *b*, and the colour at each point represents the magnitude of the wavelet coefficient $C(a, b)$ with black denoting a value close to zero through red to white denoting a large value. The range of scales for each picture has been chosen so that in each case the main information has been captured: thus, for the lowest (5 kHz) frequency signals, it is necessary to choose a larger range of scales than for the higher (18kHz and 25 kHz) frequency signals because the former signals contain information at higher scales (equivalently, lower frequencies). It is clear that some of the features in the CWT can be given a “physical” interpretation, as follows.

The presence of large coefficients at very small scales (very high frequencies) and for the duration of the signals would appear to correspond to measurement noise in the signal. This is most apparent in the CWT of the 5 kHz signal shown in Figure 13.[6]

The presence of large coefficients at small scales (equivalently, high frequencies) would appear to correspond to specific “events” in the signal: the turning on and turning off of the device, and the arrival of reflections. These are most apparent in the pictures shown in Figure 14. The turning on of the device near to the start of the signal followed a short time later by the arrival of a reflection are clearly visible. As expected, this reflection is absent from the pictures of Figure 13, although the arrival of a reflection much later, and near the end of the signal, may be seen.

Recall that the drive signal for the underlying measurements is a discrete-frequency tone-burst of finite duration. In fact, the drive signal lasts for a fixed number of cycles and, consequently, its duration (in time) depends on its frequency, becoming shorter as the frequency is increased. This explains the presence of an additional event near to the end of the 25 kHz signals, which we interpret as corresponding to the device being turned off.

The presence of large coefficients at high scales (low frequencies) would appear to correspond to the steady-state and resonant behaviour of the device. The main set of “ovals” represents the undamped sinusoidal (steady-state) component of the signal. For the three drive frequencies, these ovals occur at:

a) different scales, which perhaps gives a clue as to how “scale” may be related *quantitatively* as well as *qualitatively* to “frequency”, and

b) different time intervals, which is another indication of the different drive frequencies.

[6] In the display of the CWTs, the colour-maps are set automatically so that “black” represents the minimum CWT coefficient and “white” the maximum. For this reason it is not possible to compare directly the ranges of values of coefficients for the CWTs shown. Furthermore, it is for this reason that the effect described here is most visible for the 5 kHz signal of Figure 13: the range of values of coefficients is much smaller in this particular case.

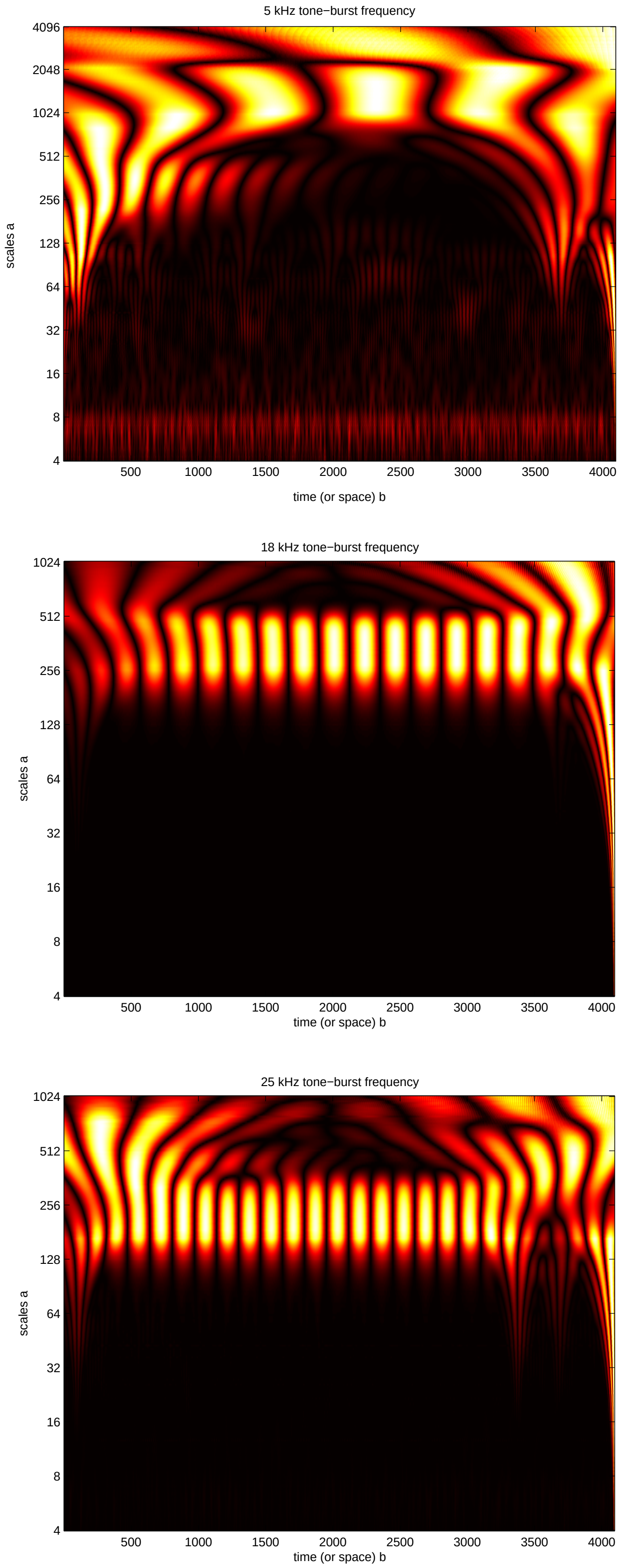


**Figure 13**: Representation of the CWT (using the Morlet wavelet) of the waveforms in Figure 2: (a) 5 kHz, (b) 18 kHz, and (c) 25 kHz drive frequencies.

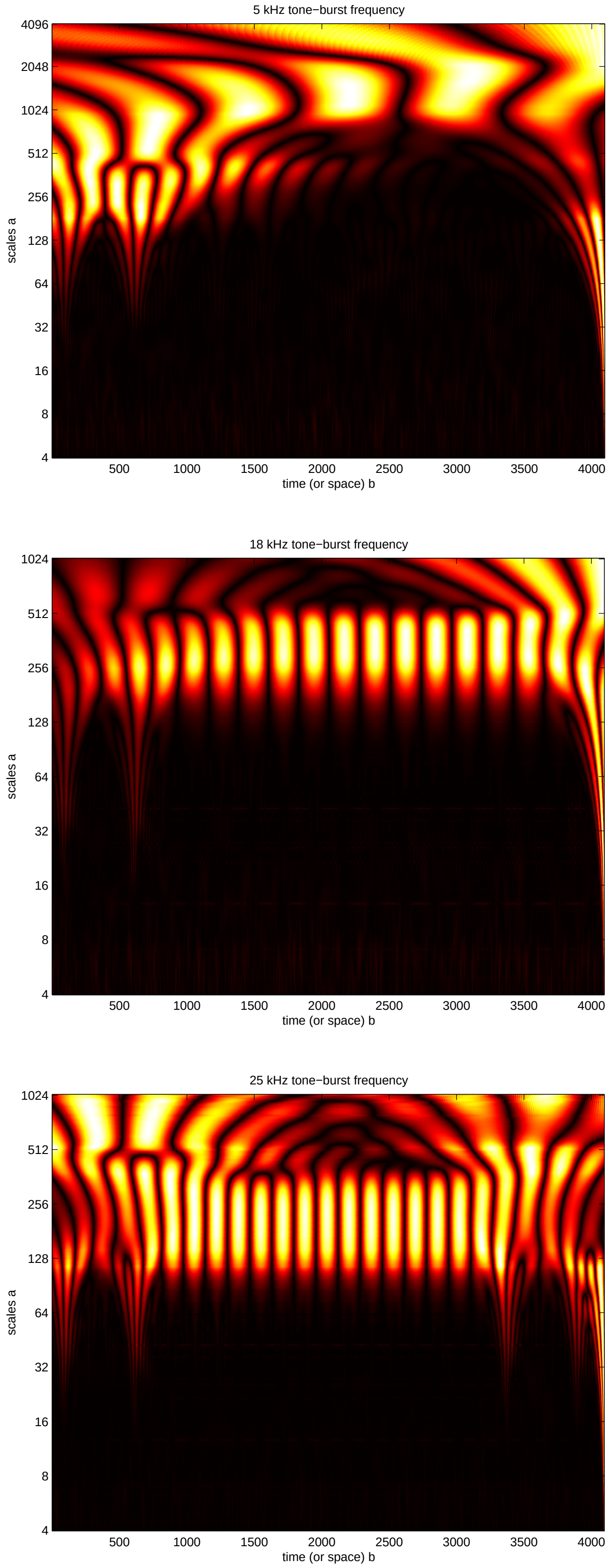


**Figure 14**: Representation of the CWT (using the Morlet wavelet) of the waveforms in Figure 3: (a) 5 kHz, (b) 18 kHz, and (c) 25 kHz drive frequencies.

In addition, for the 5 kHz and 25 kHz signals we observe subsidiary sets of "oval" features that represent the damped sinusoidal (resonant) component of the signals. These ovals occur:

a) close to when the device is turned on and off and the arrival of reflections identified before, and

b) at approximately the same scales for all three drive signals.

The CWT would appear to be useful tool for providing qualitative information about signals of the type arising in the acoustics application considered here. It would appear harder, however, to derive quantitative information, particularly as there is some "merging together" of the features discussed above. For example, it is difficult to separate completely in the CWT pictures information relating to the steady-state part of the signal from that relating to the resonant part.

Another complication would appear to be the choice of wavelet for computing the CWT. The Morlet wavelet considered here is just one of a large number of wavelets and wavelet families. Different wavelets have different properties (see, e.g., [7]) in terms of their support, symmetry, regularity, etc. For the acoustic application considered in this report, we have generally used wavelets having a high degree of regularity as this property helps produce smooth reconstructed signals. Our experience is that other choices of wavelet can be less successful in making clear features, such as when the device is turned on and off and the arrival of reflections, in the underlying signals.

### *3.1.2 Discrete wavelet transform*

In a discrete wavelet transform (DWT), the scale parameter *a* and translation parameter *b* are restricted to integer values only. In the majority of cases, the choice of *a* and *b* is limited to the discrete set:

$$(j,k) \in Z^2, \qquad a = 2^j, \qquad b = k2^j = ka,$$

where $Z$ denotes the set of integers. The parameters *a* and *b* are replaced by the indices *j* and *k* so that equation (7) becomes

$$C(j,k) = 2^{-j/2} \int f(t)\, \overline{\Psi\left(2^{-j} t - k\right)}\, \mathrm{d}t.$$

Provided the mother wavelet satisfies certain conditions, perfect reconstruction of a signal from its DWT is possible, with a reconstruction formula analogous to equation (8).

From a signal processing point of view, the DWT can be thought of as combining low- and high-pass filters $\mathcal{G}$ and $\mathcal{H}$ with a decimation operator $\mathcal{D}$ which selects alternate members of the sampled signal to obtain new filters $\mathcal{G}_0 = \mathcal{D}\mathcal{G}$ and $\mathcal{H}_0 = \mathcal{D}\mathcal{H}$. Applying $\mathcal{G}_0$ and $\mathcal{H}_0$ to a discrete signal of length $N$ gives rise to two signals, both of length $N/2$: a signal *D1* which conveys *detail* in the original signal, and a signal *A1* which *approximates* the original signal.

By repeating this decomposition process, with successive approximations being decomposed in turn, the original signal is broken down into many lower-resolution components. This process is illustrated schematically in Figure 15. Figure 16 shows the reconstruction of the signal *S* from its 3-level decomposition. The highest level approximation coefficients (in this case *A3*) and the detail coefficients *D1*, *D2* and *D3* are all that are required for the reconstruction.

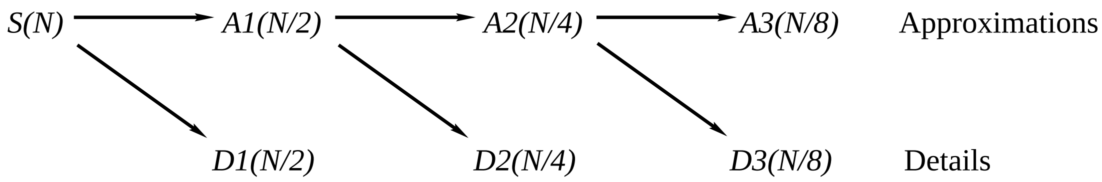


**Figure 15**: Schematic view of a 3-level decomposition of a signal *S* into approximation coefficients *A3* and detail coefficients *D1*, *D2* and *D3*. In parentheses is indicated the length of each sequence, e.g., the approximation *A3* has length *N*/8.

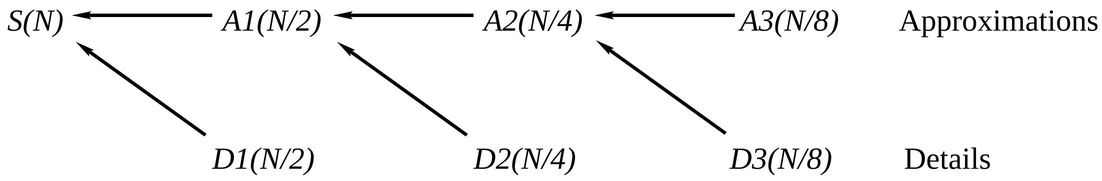


**Figure 16**: Schematic view of the reconstruction of a signal *S* from its 3-level decomposition.

One way of visualising the DWT is to plot the detail coefficients at each level. Figure 17 shows a DWT of three of the waveforms shown in Figures 2 and 3, viz., the 5 kHz and 25kHz waveforms from Figure 2 and the 5 kHz waveform from Figure 3. The transform is based on the choice of the Daubechies 3 wavelet (written as *db*3) for the mother wavelet.[7] In these plots the vertical axis corresponds to the level of decomposition or scale, the horizontal axis to translation, and the height of each vertical bar is proportional to the size of the corresponding DWT coefficient.[8]

This view of the DWT is very "efficient" (equivalently, least redundant) in terms of the number of coefficients displayed (which is of the order of the number of points in the original signal). However, it is difficult to give physical interpretation to the results: the detail at the lower levels might be interpreted as corresponding to measurement noise, but it is not clear how to associate the information at higher levels with the damped and undamped components of the signals or to extract information about the various events that are present in the signals.

Another way of visualising the DWT is to show the reconstructed approximations and details at each level. This view is much less efficient in terms of the number of coefficients displayed because *each* reconstructed approximation and detail is represented by a number of points equal to the number in the original signal. Figures 18 and 19 illustrate the processes of reconstructing the level 3 approximation *A3* and detail *D3* by undertaking a level 3 decomposition of a signal followed by a reconstruction from modified approximation and detail coefficients. The results of the repeated application of these processes to the 5 kHz waveform from Figure 2 to obtain the approximations and details down to level 10 are shown in Figures 20 and 21, respectively. As above the DWT decomposition is based on the *db*3 wavelet. This view is a little more useful. The details give some information about the locations of events (near the start and end of the details at levels 5 and 6) but it is still difficult to discriminate between the damped and undamped components of the signal.

---

[7] We use here the notation *dbN* for the Daubechies wavelet of order *N*. Some authors use 2*N* instead of *N*.

[8] For the purposes of visualisation the coefficients at each level have been scaled.

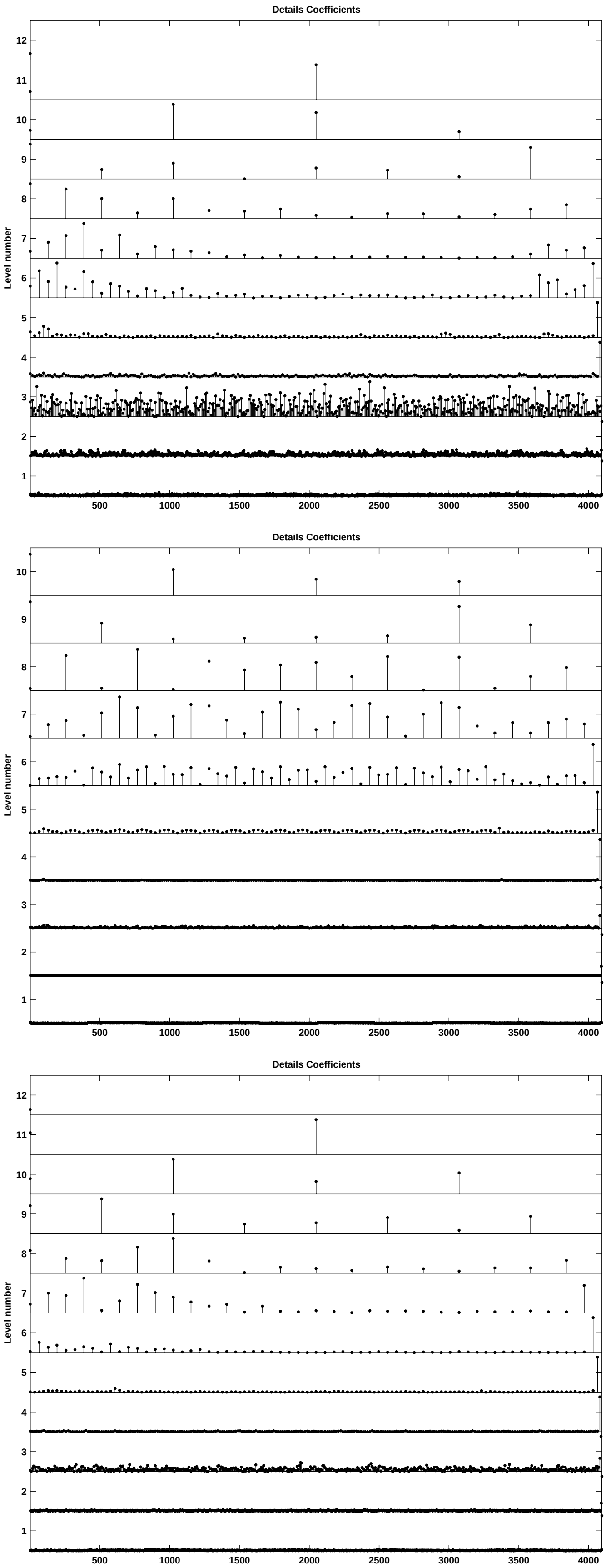


**Figure 17**: Representation of the detail coefficients generated by the DWT of the 5 kHz and 25 kHz waveforms from Figure 2 and the 5 kHz waveform from Figure 3. The wavelet for the DWT is *db*3.

Decomposition

$$\begin{tikzcd}
S(N) \arrow[r] \arrow[dr] & A1(N/2) \arrow[r] \arrow[dr] & A2(N/4) \arrow[r] \arrow[dr] & A3(N/8) & \text{Approximations} \\
& D1(N/2) & D2(N/4) & D3(N/8) & \text{Details}
\end{tikzcd}$$

Set all detail coefficients to zero

$$D1(N/2) \longrightarrow 0(N/2)$$
$$D2(N/4) \longrightarrow 0(N/4)$$
$$D3(N/8) \longrightarrow 0(N/8)$$

Reconstruction

$$\begin{tikzcd}
U(N) & C1(N/2) \arrow[l] & C2(N/4) \arrow[l] & A3(N/8) \arrow[l] & \text{Approximations} \\
& 0(N/2) \arrow[ul] & 0(N/4) \arrow[ul] & 0(N/8) \arrow[ul] & \text{Details}
\end{tikzcd}$$

**Figure 18**: Schematic view of the reconstruction of the approximation *A3* from its 3-level decomposition.

Decomposition

$$\begin{tikzcd}
S(N) \arrow[r] \arrow[dr] & A1(N/2) \arrow[r] \arrow[dr] & A2(N/4) \arrow[r] \arrow[dr] & A3(N/8) & \text{Approximations} \\
& D1(N/2) & D2(N/4) & D3(N/8) & \text{Details}
\end{tikzcd}$$

Set level 3 approximation coefficients, level 2 and level 1 detail coefficients to zero

$$D1(N/2) \longrightarrow 0(N/2)$$
$$D2(N/4) \longrightarrow 0(N/4)$$
$$A3(N/8) \longrightarrow 0(N/8)$$

Reconstruction

$$\begin{tikzcd}
V(N) & F1(N/2) \arrow[l] & F2(N/4) \arrow[l] & 0(N/8) \arrow[l] & \text{Approximations} \\
& 0(N/2) \arrow[ul] & 0(N/4) \arrow[ul] & D3(N/8) \arrow[ul] & \text{Details}
\end{tikzcd}$$

**Figure 19**: Schematic view of the reconstruction of the detail *D3* from its 3-level decomposition.

The DWT, employed as a visualisation tool, would appear to be less useful for providing (qualitative) information about the waveforms considered in this acoustics application compared with the CWT. However, other possible uses of the DWT (e.g., for de-noising and feature identification) are considered in the following sections. As for the CWT the user is faced with a wide choice of wavelet and wavelet families on which to base the computed DWT.

## 3.2 DE-NOISING

As noted in Section 1, the signal detected by the receiving hydrophone is often contaminated by noise, potentially from both acoustic and electrical sources. The signal modelling techniques of Section 2.3 aim to *smooth* the data by constructing an estimate of the underlying signal that would be measured in the absence of measurement noise. However, the success of these techniques is to a large extent dependent on the amount of noise present in the data. Linear prediction estimators, including the classical method of Prony, are notoriously sensitive to the presence of noise [12].[9] Furthermore, the non-linear least-squares problem that the signal modelling techniques aim to solve is often poorly conditioned, and as a consequence the performance of algorithms for solving this problem tends to degrade as the noise level is increased.

One possible application of wavelet analysis is *de-noising* the signal prior to using the signal modelling techniques. Consider a signal described by measurements $\{y_i: i = 1, \ldots, m\}$ subject to errors $\{\varepsilon_i: i = 1, \ldots, m\}$ that are assumed to be drawn from a Gaussian distribution with mean zero and variance $\sigma^2$. It is shown [17] that the coefficients in a discrete wavelet decomposition of the signal are themselves subject to errors drawn from a Gaussian distribution with mean zero and variance $\sigma^2$. This result is used as the basis of de-noising the signal: only "large" coefficients are assumed to contain information about the signal while "small" coefficients are attributed to noise in the signal values. De-noising involves keeping only those coefficients with magnitudes greater than a certain threshold $\lambda$ while setting all other (small) coefficients to zero. The de-noising procedure is described schematically in Figure 22.

There are two main types of thresholding strategies:

1. *hard* thresholding in which coefficients $D(j, k)$ having magnitudes less than or equal to a threshold $\lambda$ are set to zero, with all other coefficients left unchanged, i.e.,

$$E(j,k) = \begin{cases} D(j,k) & \text{if } |D(j,k)| > \lambda, \\ 0 & \text{otherwise,} \end{cases}$$

   and

2. *soft* thresholding in which coefficients $D(j, k)$ with magnitudes less than or equal to a threshold $\lambda$ are set to zero, with other coefficients "shrunk towards zero", i.e.,

$$E(j,k) = \operatorname{sign}\{D(j,k)\}\max\{0, |D(j,k)| - \lambda\}.$$

[9] Indeed a variety of methods based on the original Prony algorithm, using for example forward and backward error prediction and subset selection based on singular value matrix decomposition, have been proposed to overcome this sensitivity.

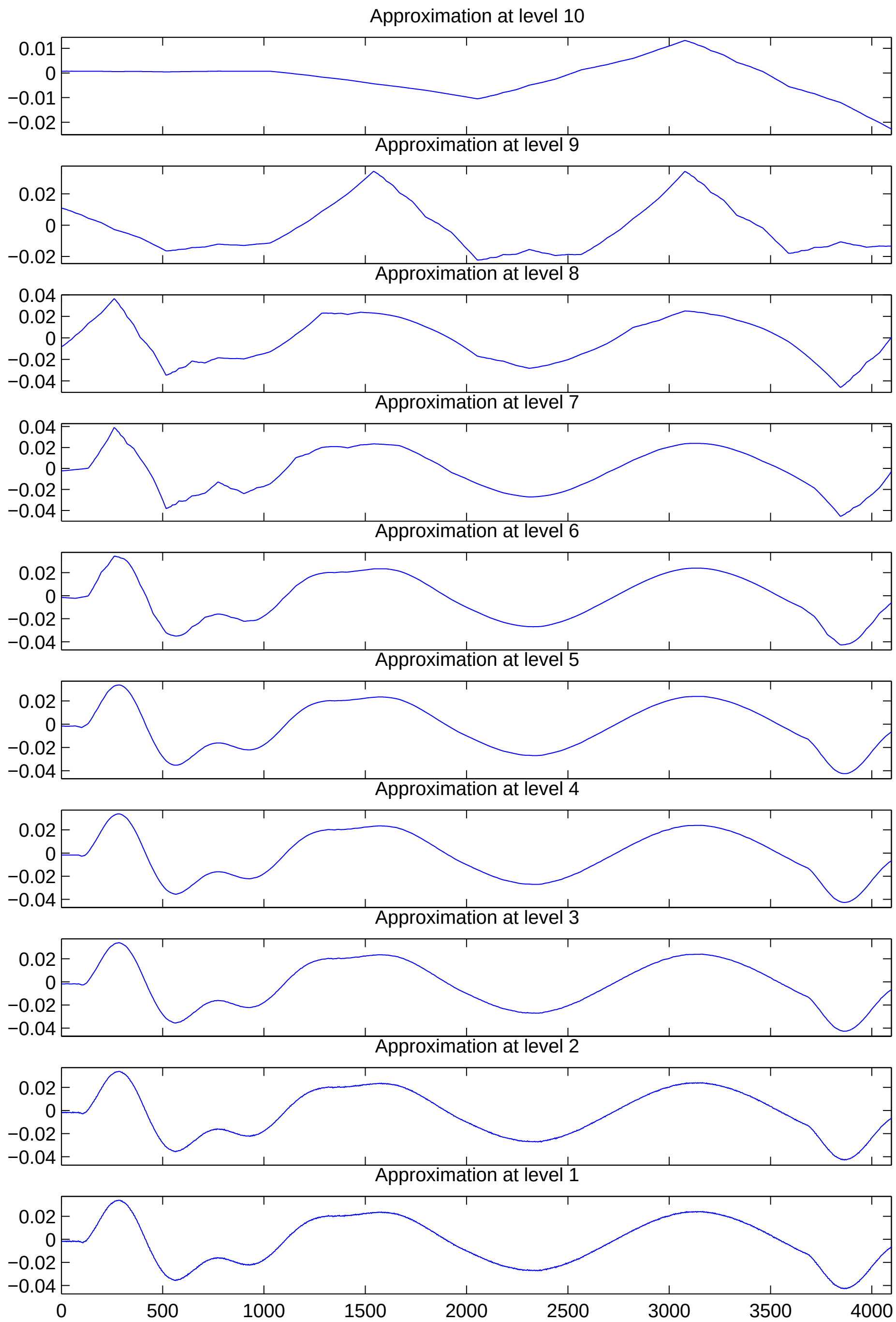


**Figure 20**: Reconstructed approximations for the 5 kHz signal from Figure 2. The wavelet for the DWT is *db*3.

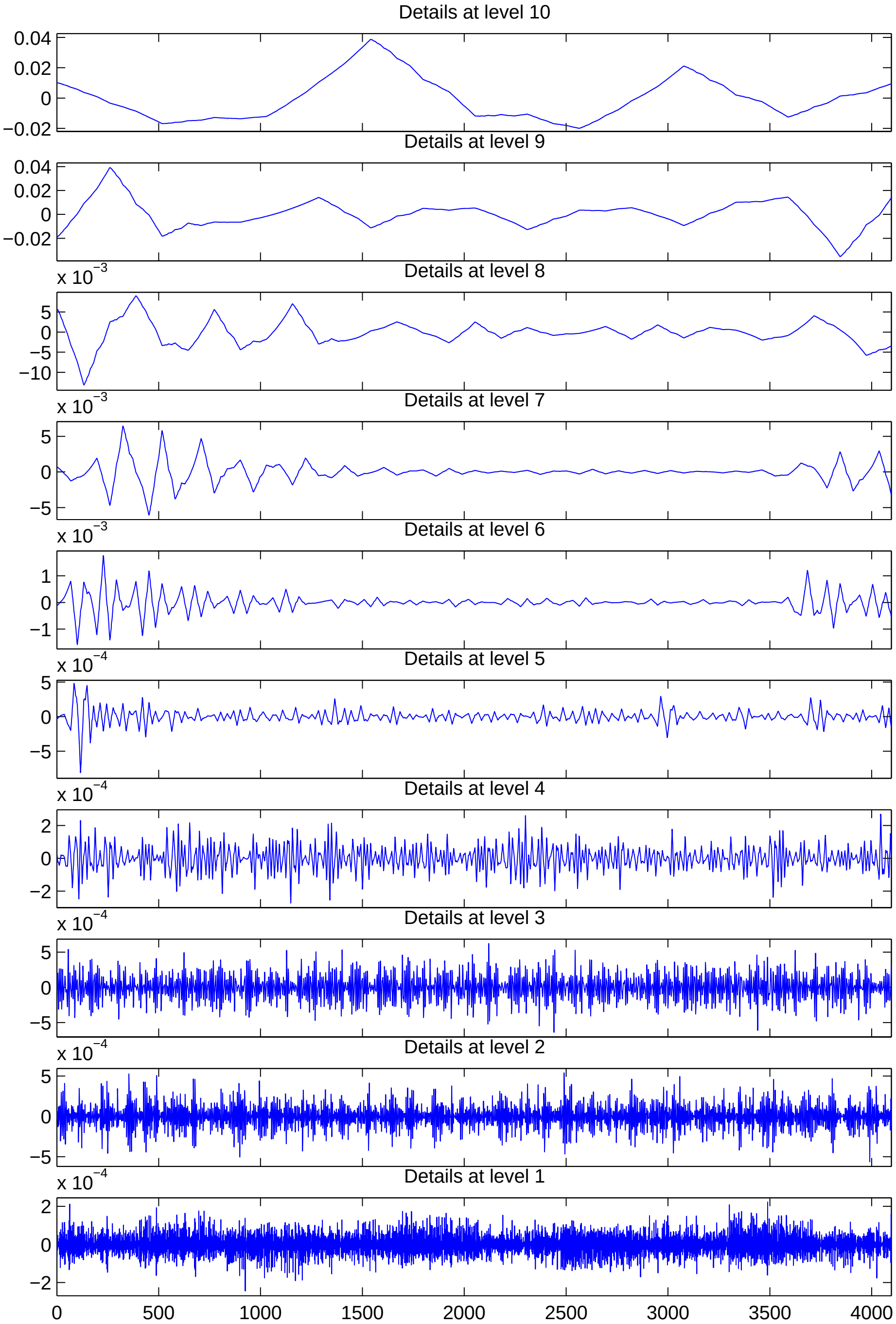


**Figure 21**: Reconstructed details for the 5 kHz signal from Figure 2. The wavelet for the DWT is *db*3.

Decomposition

$$\begin{tikzcd}
S(N) \arrow[r] \arrow[dr] & A1(N/2) \arrow[r] \arrow[dr] & A2(N/4) \arrow[r] \arrow[dr] & A3(N/8) & \text{Approximations} \\
& D1(N/2) & D2(N/4) & D3(N/8) & \text{Details}
\end{tikzcd}$$

Thresholding of detail coefficients

$$\begin{tikzcd}
D1(N/2) \arrow[r] & E1(N/2) \\
D2(N/4) \arrow[r] & E2(N/4) \\
D3(N/8) \arrow[r] & E3(N/8)
\end{tikzcd}$$

Reconstruction

$$\begin{tikzcd}
T(N) & B1(N/2) \arrow[l] & B2(N/4) \arrow[l] & A3(N/8) \arrow[l] & \text{Approximations} \\
& E1(N/2) \arrow[ul] & E2(N/4) \arrow[ul] & E3(N/8) \arrow[ul] & \text{Details}
\end{tikzcd}$$

**Figure 22**: Schematic view of the procedure of de-noising a signal *S* using its 3-level decomposition.

There are many methods for choosing the threshold value (see, e.g., [7]). The de-noising carried out for this report uses soft thresholding with a fixed form threshold value [17] given by

$$\hat{\sigma}\sqrt{2\log N},$$

where $\hat{\sigma}$ is an estimate of the variance of the measurement noise $\sigma$ and $N$ is the number of data points in the waveform. The estimate $\hat{\sigma}$ is obtained by a robust procedure and is calculated in terms of the absolute deviations of the wavelet coefficients from the median of the coefficients [7].

The de-noising process is illustrated here using the 5 kHz waveform of Figure 2. The DWT (based on *db*3) for this waveform is shown at the top of Figure 17, and the modified DWT after application of a thresholding strategy at the top of Figure 23. A large number of coefficients are set to zero, especially those corresponding to high frequency (low level numbers). Figure 23 also shows the resulting de-noised waveform obtained by reconstruction from the modified coefficients. Figures 24, 25 and 26 show, respectively, the original and de-noised waveforms and the residual deviations between the two for each of the three waveforms in Figure 2.

We see from these figures that, excepting near the ends of the waveforms, the nature of the residual deviations for the three waveforms is comparable in terms of their “size” and the random behaviour exhibited. De-noising of the signals would appear to work in the sense of providing a version of the signal for subsequent analysis that is closer to being noise free. However, the benefit to the signal modelling approaches to analysing the signals is less obvious: although the performance of the numerical methods used in these approaches can be different for a de-noised signal compared to the original signal[10], the final results are often very similar for the two signals.

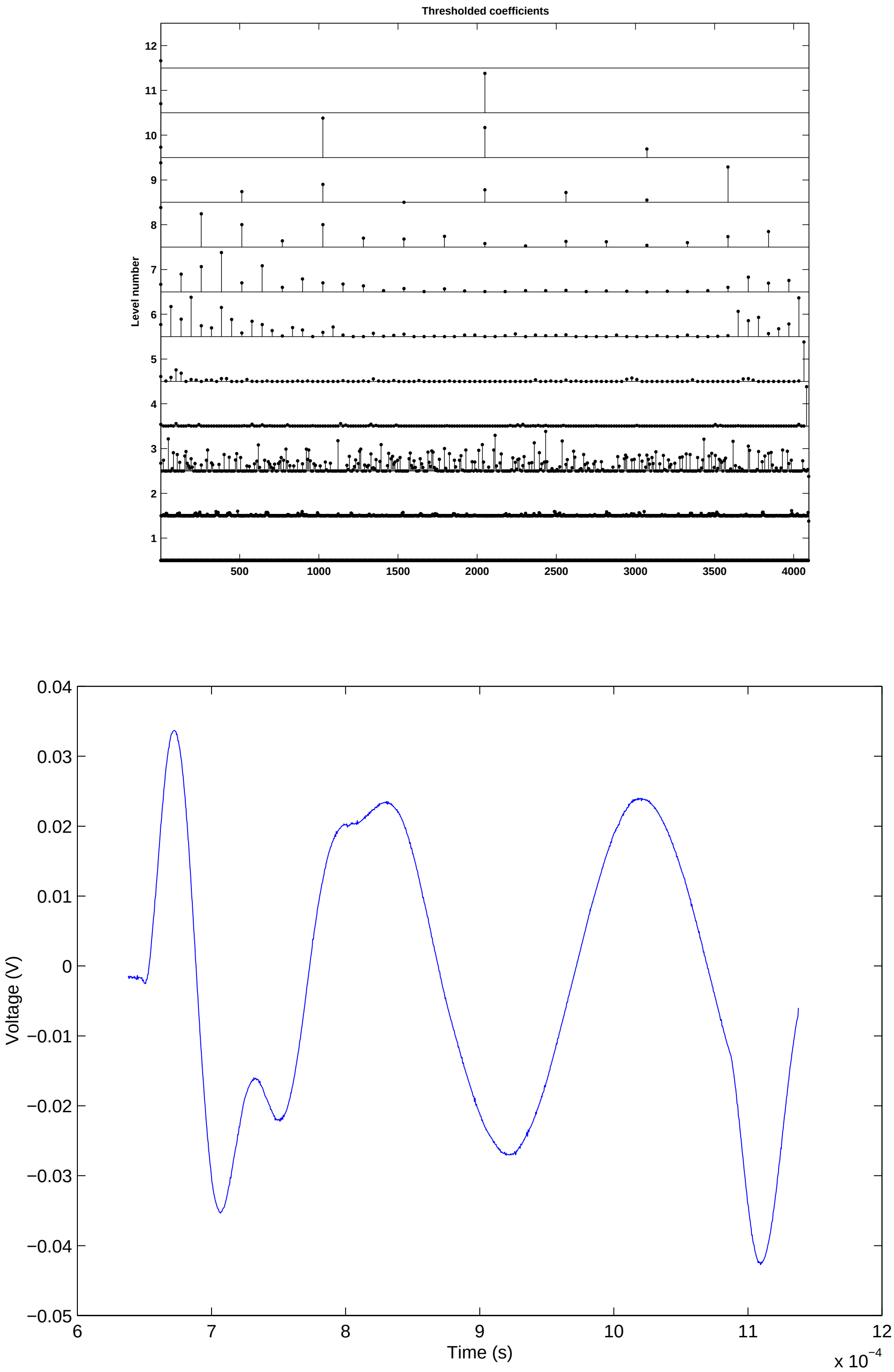


**Figure 23**: Coefficients of the DWT (using *db*3) of the 5 kHz waveform from Figure 2 after thresholding, and the resulting de-noised waveform.

[10] For example, the numerical methods used might converge for the de-noised data using a model with two resonance components but might fail to do so for the original data.

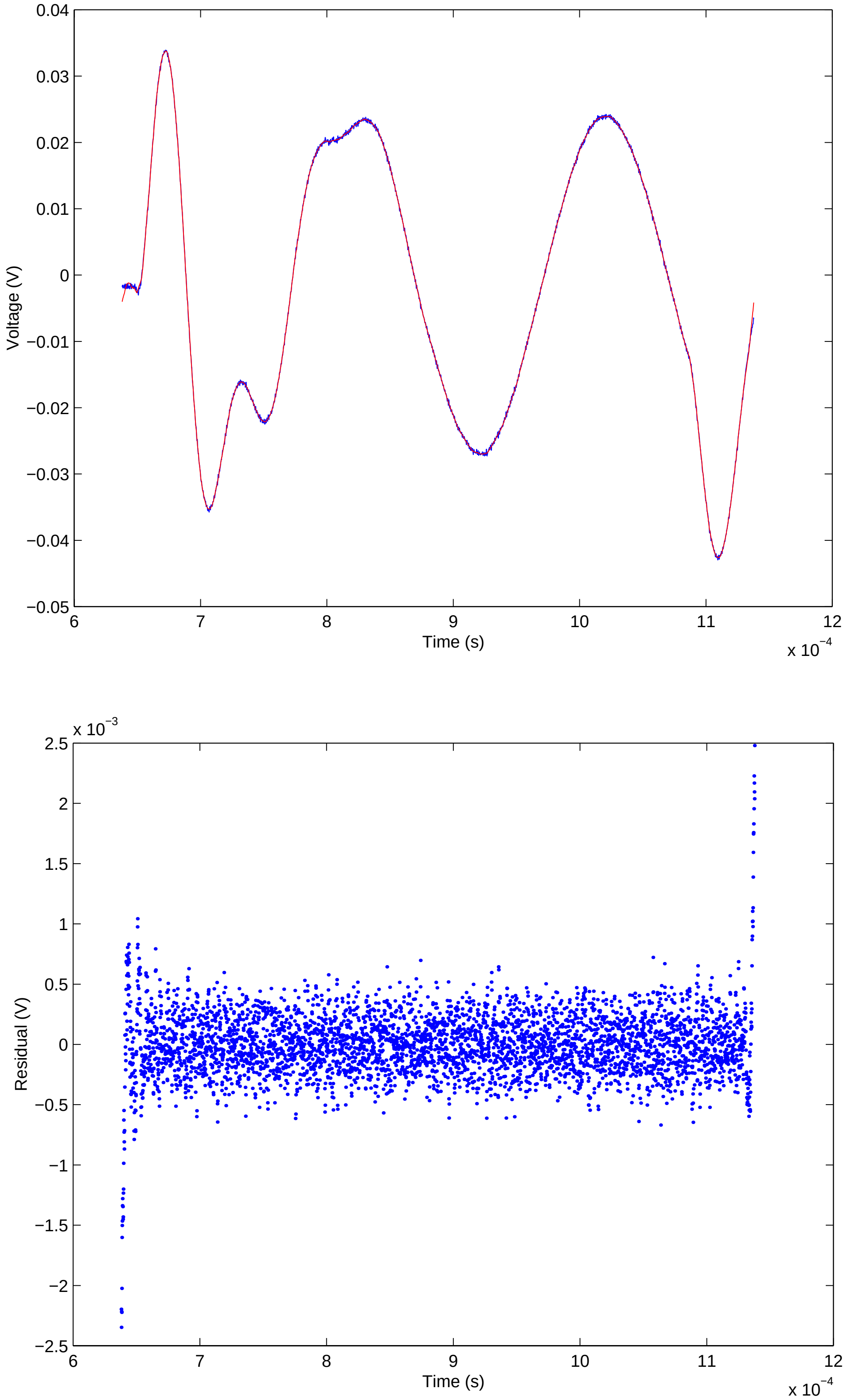


**Figure 24**: The 5 kHz waveform from Figure 2 plotted against the waveform after de-noising, and the residual deviations between the two waveforms.

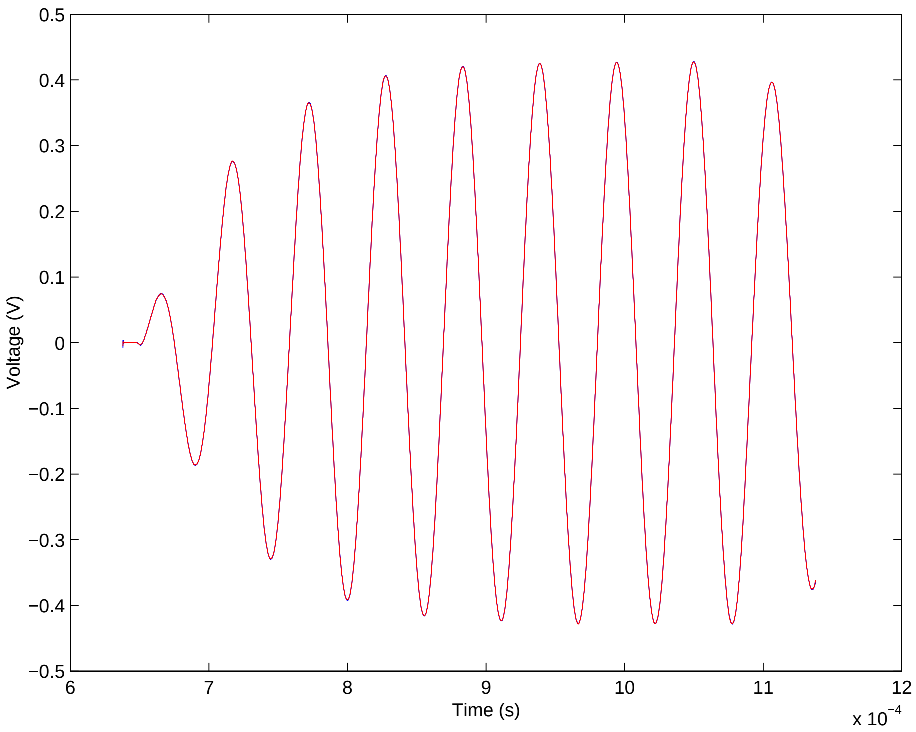


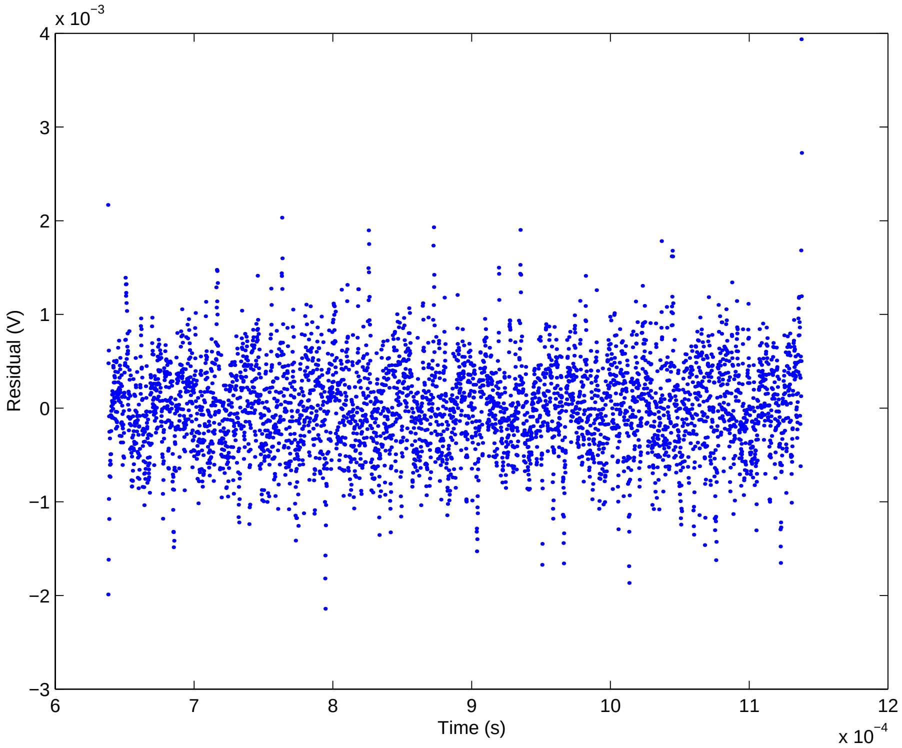


**Figure 25**: The 18 kHz waveform from Figure 2 plotted against the waveform after de-noising, and the residual deviations between the two waveforms.

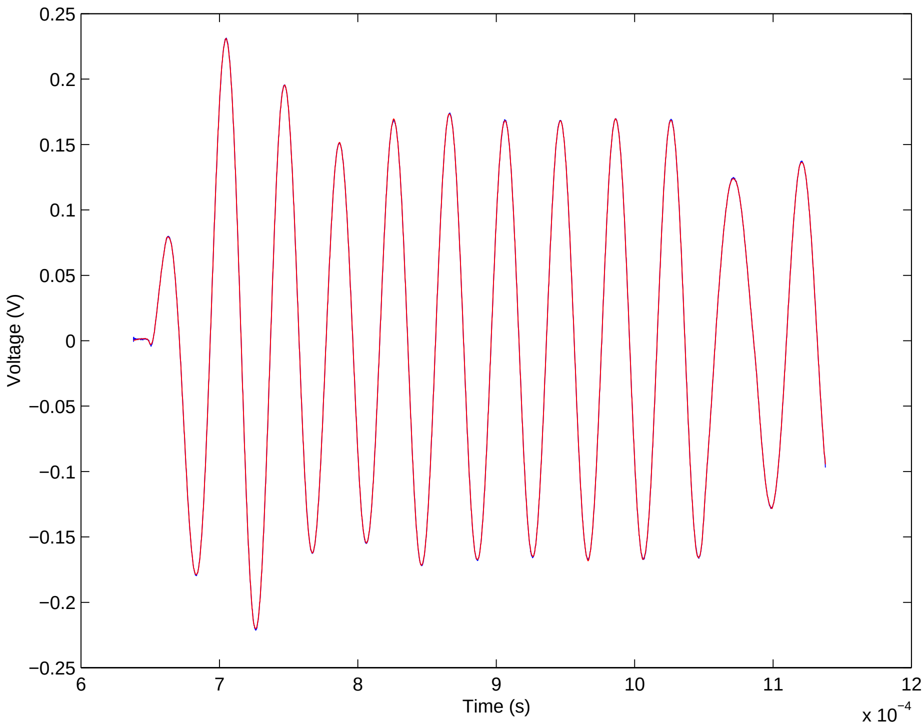


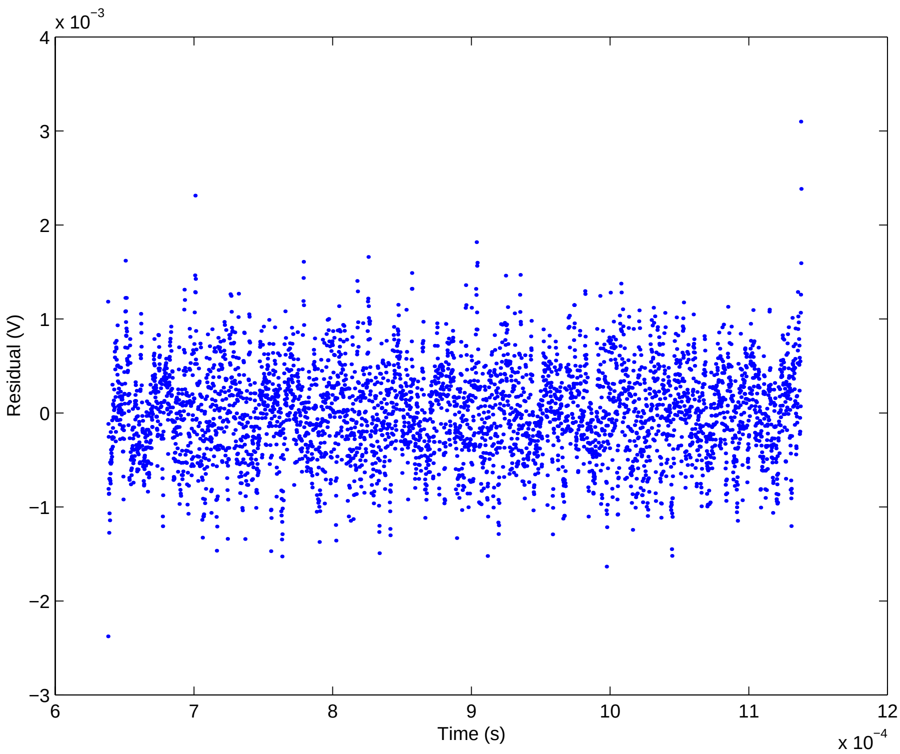


**Figure 26**: The 25 kHz waveform from Figure 2 plotted against the waveform after de-noising, and the residual deviations between the two waveforms.

## 3.3 FEATURE IDENTIFICATION

One of the first applications of wavelets was in the analysis of seismic data where wavelets were used for the detection of events that are localised in time or frequency or both. Identification of events or *features* in signals is possible since the size of a wavelet coefficient provides information about whether there is a change in the signal at a given point in time and at a given scale. Consequently, a possible use of wavelets in the analysis of the acoustic signals considered in this work is for the identification from a measured waveform of the times of arrival at the receiving hydrophone of the direct signal and of reflections.

The accurate estimation of these times is useful for a number of reasons:

1. When applying the methods that make use of data within the echo-free time (Section 2.2), it is beneficial to maximise the chosen echo-free time so that the maximum amount of data is made available for these methods.

2. The signal modelling techniques applied to data measured in a reverberant field (Section 2.3.2) tend to perform better when the arrival times are treated as (known) fixed parameters rather than as free parameters to be determined as part of the optimisation.

3. It is possible to verify the estimates of these times obtained from other means (such as from the measurement of the positions of the devices within the tank and knowledge of the speed of the acoustic wave within the medium contained in the tank).

Visualisation of the continuous wavelet transform (CWT) of a signal provides a general means of identifying a feature or features within a particular signal (Section 3.1). This is illustrated clearly in Figures 13 and 14 where, e.g., the presence of large coefficients at small scales and at isolated times would appear to correspond to the turning on and turning off of the device, and the arrival of reflections.

Consider the CWT visualisations shown in Figure 14 corresponding to the signals of Figure 3. One feature that can be identified in all three graphs is centred (approximately) on data point 630 and between scales 32 and 128. This feature corresponds to the arrival of the first reflection.[11] The top graphs of Figures 27 and 28 show some of the detail of the CWT for the 18 kHz signal. The graph in Figure 27 shows the CWT between scales 32 and 128, and that in Figure 28 shows the part of the CWT between points 550 and 700. In Figure 29 we present sections of the CWT shown in Figure 27 at scales 128, 96, 64 and 32, respectively.

An approach to obtaining an estimate of the arrival time for the reflection is as follows: select a value for the scale and a time interval which is believed to contain the arrival time, and determine the time within the interval at that scale for which the CWT coefficient has greatest magnitude. The bottom graphs of Figures 27 and 28 show the positions at each scale of the CWT coefficients that define local minima and maxima.[12] The arrival time for the reflection is estimated by the local maxima at the "centre" of the feature associated with this event: this is the third "curve" in the bottom graph of Figure 28 to which the other curves associated with the event appear to converge.

Applying this approach, for the waveform corresponding to the 18 kHz signal of Figure 3 the arrival time is estimated as occurring at point 628 (approximately 76.65 μs after the start of

[11] The feature is not present in the CWTs of Figure 13 corresponding to the signals of Figure 2 for which the first reflection is known to arrive much later.

[12] The positions of local minima and maxima are determined at the highest scale (128) and the variation of these positions with scale is displayed.

signal) for scale 32, and at point 647 (78.97 μs after the start of signal) for scale 128. It is known that the turning on of the device occurs at (approximately) 12.33 μs after the start of the signal, so the echo-free time is estimated by 64.32 μs (for scale 32) and 66.64 μs (for scale 128). For the other waveforms (corresponding to the 5 kHz and 25 kHz signal, respectively), the corresponding ranges are [64.08, 66.64] μs and [64.45, 65.91] μs. An analysis that uses information about the positions of the devices within the tank (relative to each other and the reflecting surfaces) suggests that the echo-free time is approximately 66.40 μs.[13]

The use of the discrete wavelet transform (DWT) in feature analysis is widespread [3, 4]. Figure 30 shows the reconstructed level 5 detail coefficients[14] for the three signals in Figure 3 obtained using the wavelet *db*3. This particular wavelet is chosen because it has short support, and so can be expected to be good for providing time-localised information. The particular detail level is chosen because, at least for the 5 kHz and 18 kHz frequencies, the event of interest appears to be easily identified.[15] The information provided by the DWT is used to estimate the arrival time for the reflection in the following way: the position within a prescribed (time-)window[16] of the DWT coefficient of maximum magnitude is determined. This approach is similar to that using the CWT but with "scale" replaced by "detail level".

Table 1 summarises the estimates of the echo-free time obtained for a number of tone-burst frequencies using the methods described above that employ the DWT and CWT. The table also includes estimates obtained from

a) the DWT but based on choices of wavelet other than *db*3,

b) dimensional information about the experimental set-up, and

c) the signal modelling approach of Section 2.3.2 in which the arrival-time is a parameter to be estimated from the data fitting problem.

| Tone-burst frequency (kHz) | DWT | | | CWT | Dimensional measurement (μs) | Signal modelling (μs) |
|---|---|---|---|---|---|---|
| | *db*3, level 5 (μs) | *db*5, level 5 (μs) | *db*7, level 5 (μs) | Morlet, scale 32 (μs) | | |
| 5 | 64.33 | 62.50 | 61.52 | 64.08 | 66.40 | 75.06 |
| 10 | 64.33 | 63.59 | 61.52 | – | 66.40 | 55.45 |
| 15 | 64.33 | 63.72 | 61.40 | – | 66.40 | 58.16 |
| 18 | 64.33 | 63.72 | 61.40 | 64.32 | 66.40 | 58.41 |
| 20 | 64.33 | 63.59 | 61.40 | – | 66.40 | 58.61 |
| 25 | 68.23 | 63.72 | 61.52 | 64.45 | 66.40 | 57.60 |

**Table 1**: Estimates of echo-free time obtained using DWT, CWT, dimensional measurement, and signal modelling techniques for waveforms corresponding to various tone-burst frequencies.

[13] The analysis assumes that the devices are point sources, and so is likely to overestimate (slightly) the "true" echo-free time.
[14] These detail coefficients are reconstructed by the procedure illustrated in Figure 19 and described in Section 3.1.2.
[15] The fact that the event is not easily identified for the (higher) 25 kHz signal suggests that it may be difficult to "automate" a procedure for providing information about the event.
[16] This window is defined by points 500 and 1000 for the results presented.

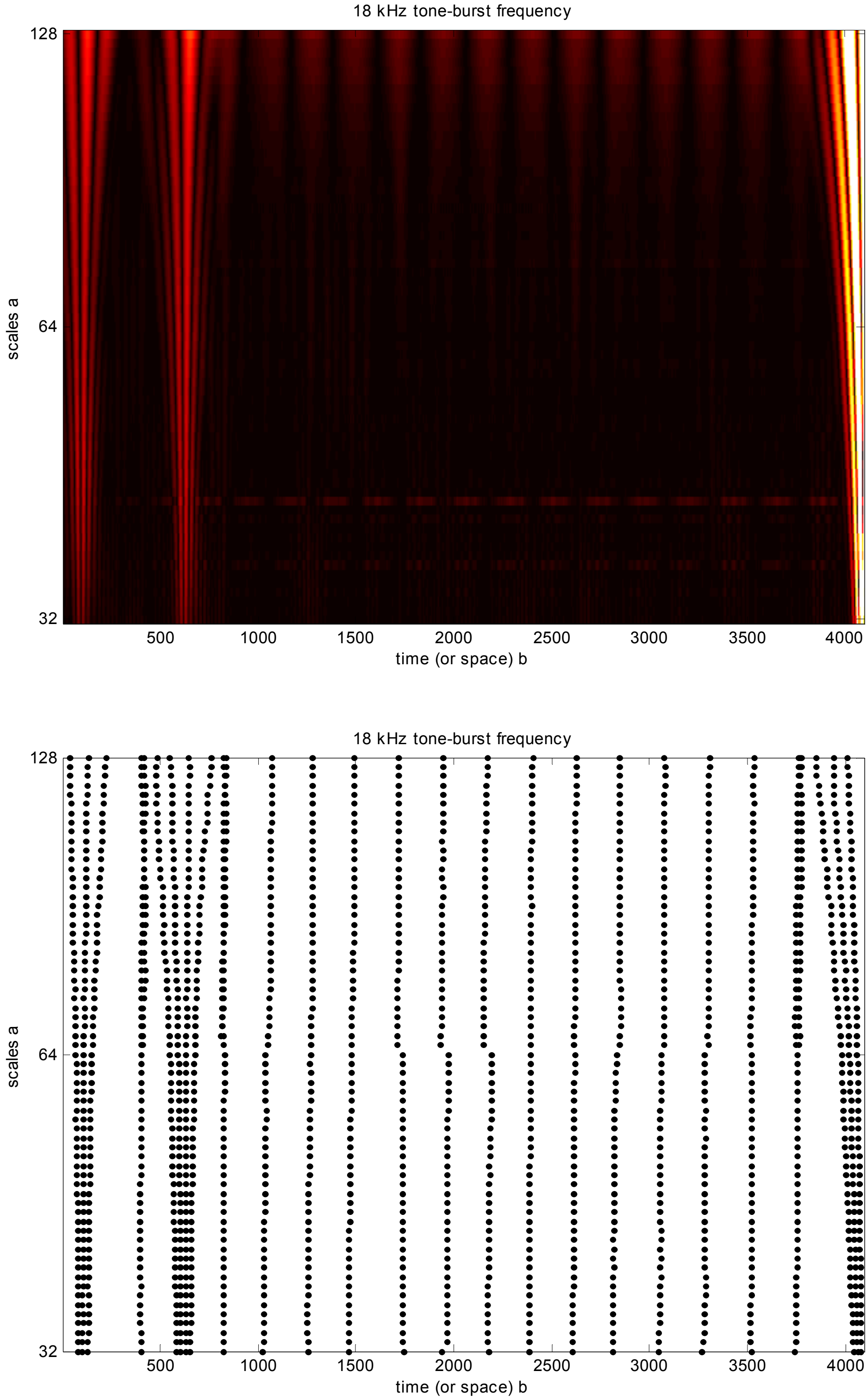


**Figure 27**: Top figure shows the CWT for the 18 kHz signal of Figure 3 between the scales 32 to 128. Bottom figure shows the (time) positions of maximum and minimum CWT coefficients as a function of scale.

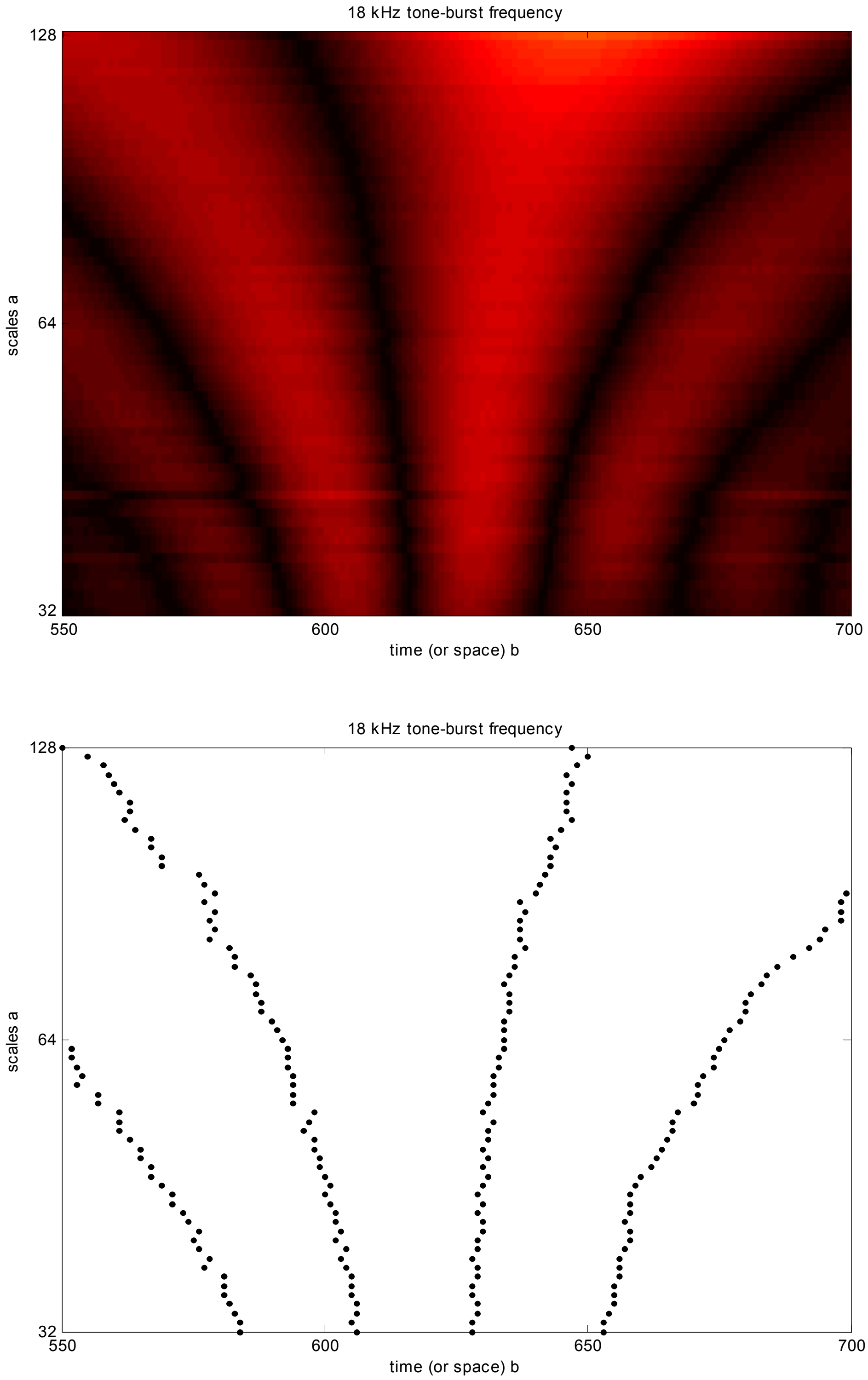


**Figure 28**: As Figure 27, but restricted to points 550 to 700.

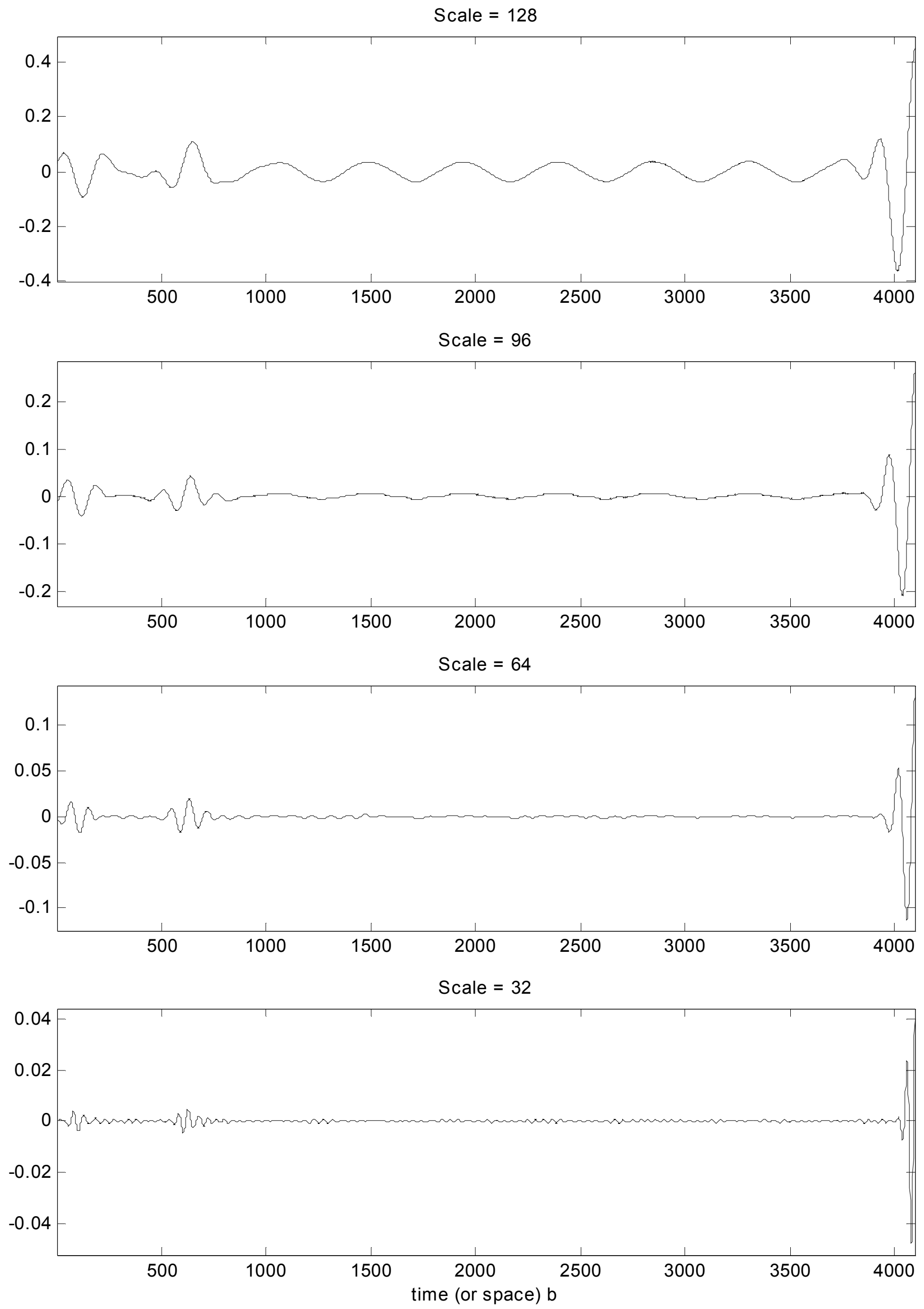


**Figure 29**: Sections of the CWT shown in Figure 27 at scales 128, 96, 64 and 32, respectively.

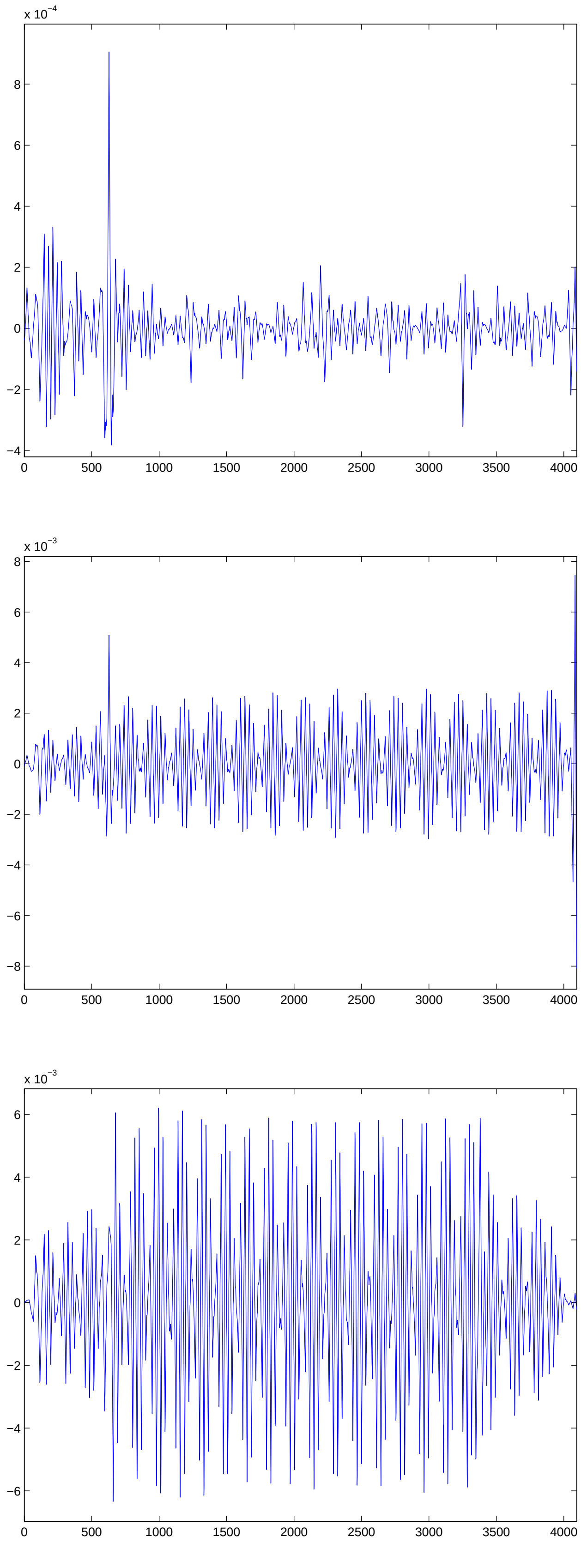


**Figure 30**: Reconstructed level 5 detail for the 5 kHz, 18 kHz and 25 kHz signals of Figure 3 obtained from the DWT based on the wavelet *db*3.

If we regard the dimensional measurement as providing a result that is reliable, it is clear that the estimates provided by the signal modelling approach are least accurate. In particular, for the lowest tone-burst frequency of 5 kHz, the echo-free time is considerably over-estimated. The methods based on the CWT and DWT would appear to provide useful quantitative information about the echo-free time. However, the results are influenced both by the choice of wavelet and the scale (for the CWT) or detail level (for the DWT), and so some user interaction is likely to be necessary to ensure sensible results.

## 4 CONCLUSIONS AND FUTURE WORK

In the calibration of underwater electroacoustic transducers undertaken in reverberant laboratory tanks, data processing is used to extract from the measured data the required information for the calibration. This information is the voltage that would be measured in the absence of contaminating effects including transients due to the resonances of the devices, reflections of the transmitted signal, and noise.

We have described a number of "traditional" approaches to performing the data analysis currently in use, including the application of signal processing techniques based on Fourier analysis as well as regression modelling. Wavelet analysis provides another approach to analysing spectrally varying sequences of data that complements traditional Fourier analysis. We have given a brief introduction to wavelet analysis, and considered how methods of analysis based on wavelets can be applied to this particular measurement problem. The intention has been to consider how wavelet analysis may support and complement the traditional methods of analysis by addressing some of the limitations of those methods and we hope that this report is useful in documenting the processes we used to obtain some useful results.

We have seen the merits of both continuous and discrete wavelet analysis. The redundancy of the CWT allows a visualisation that makes trends and features straightforward to detect and, in general, provides useful *qualitative* information about a signal. Compare, for example, the CWT and the spectrogram. The DWT, while not so useful in terms of visualisation, provides an "efficient" analysis of a signal, and is the basis for signal de-noising.

We have applied de-noising techniques based on wavelet analysis, but have found that, for the signals from the particular application considered here, the impact (on traditional analysis techniques) of such pre-processing is not strong. For other applications (in acoustics), such as that described in Appendix A, the use of de-noising may prove to be more useful.

We have used both continuous and discrete wavelet analysis as a means for detecting echoes in signals, and have found both to be useful for this application in terms of providing better information than that obtained from (traditional) signal modelling techniques.

Since starting this project, we have identified several metrology areas where wavelet techniques may prove useful, e.g., the analysis of lithotripter data in the treatment of kidney stones (Appendix A) and the characterisation of surface texture in dimensional metrology.

One area requiring further investigation is the use of complex harmonic wavelets as described by Newland [18, 19, 20]. These wavelets have simple structure and efficient implementation of a discrete transform based on the FFT can be carried out. Harmonic wavelets have been used in many engineering applications, e.g., vibration analysis, to obtain time-frequency maps for rapidly changing transient signals.

## 5 ACKNOWLEDGEMENTS

This work was supported by the Strategic Research Programme at the National Physical Laboratory.

The authors would like to thank Maurice Cox (CMSC) for reviewing this report and Catherine Bickley (CMAM) for her assistance with the lithotripter application.

## 6 REFERENCES

[1] BOBBER, R.J. *Underwater Electroacoustic Measurements*. USA, Peninsula Press, 1989 (2nd edition).

[2] DAUBECHIES, I. *Ten lectures on wavelets*, Vol 61 CBMS-NSF Regional Conference in Applied Math., SIAM, PA, 1992.

[3] COIFMAN, R., MEYER, Y., QUAKE, S. and WICKERHAUSER, M. *Signal processing and compression with wave packets*. Yale University (1990).

[4] NASON, G.P., SAPATINAS, T. and SAWCZENKO, A.. *Statistical modelling of time series using non-decimated wavelet representations*. University of Bristol, Bristol, September 1997.

[5] DAHMEN, W. *Wavelet and multiscale methods for operator equations*. Acta Numerica, pp 55-228, CUP, 1997.

[6] ROBINSON, S.P. *Review of methods for low frequency transducer calibration in reverberant tanks*. NPL Report CMAM 034, National Physical Laboratory, 1999.

[7] LORD, G.J., PARDO-IGUZQUIZA, E. and SMITH, I.M. *A practical guide to wavelets for metrology*. NPL Report CMSC 02/00, National Physical Laboratory, 2000.

[8] THE MATHWORKS, INC. *MATLAB: The Language of Technical Computing*, 2000.

[9] THE MATHWORKS, INC. *Signal Processing Toolbox User's Guide: For Use with MATLAB*, 1998.

[10] THE MATHWORKS, INC. *Wavelet Toolbox User's Guide: For Use with MATLAB*, 1996.

[11] VAN LOAN, C. *Computational Frameworks for the Fast Fourier Transform*, SIAM, PA, 1992.

[12] HARRIS, P.M. and ROBINSON, S.P. *Acoustic signal modelling and its application to the calibration of underwater electroacoustic transducers in reverberant environments*. Proceedings of the Institute of Acoustics, **20**, pt. 3, 13–20, 1998.

[13] ROBINSON, S.P. and HARRIS, P.M. *Modelling acoustic signals in the calibration of underwater electroacoustic transducers in reverberant laboratory tanks*. NPL Report CMAM 029, National Physical Laboratory, 1999.

[14] AINSLEIGH, P.L. and GEORGE, J.D. *Signal modeling in reverberant environments with application to underwater electroacoustic transducer calibration*. J. Acoust. Soc. Am., **98**, 270–279, 1995.

[15] ROBINSON, S.P. and HARRIS, P.M. *Modelling acoustic signals containing reflections in the calibration of underwater acoustic transducers in laboratory tanks*. NPL Report CMAM 052, National Physical Laboratory, 2000.

[16] LE GALL, Y. and GAUTARD, S. *Transmitting response measurement of low frequency projectors in confined environments with maximum length sequences and homomorphic signal processing*. Proceedings of the Institute of Acoustics, **20**, pt. 3, 21–28, 1998.

[17] DONOHO, D. L. and JOHNSTONE, I. M. *Ideal spatial adaptation by wavelet shrinkage*, Biometrika, **81**, 425–455, 1994.

[18] NEWLAND, D. E. *Harmonic wavelet analysis*, Proceedings R. Soc. Lond. A, **443**, 1993.

[19] NEWLAND, D. E. *Ridge and Phase Identification in the Frequency Analysis of Transient Signals by Harmonic Wavelets*, ASME J.of Vibration and Sound, **121**, 1999.

[20] NEWLAND, D. E. *Harmonic Wavelets in Vibrations and Accoustics* in "Wavelets: The Key to Intermittent Information", 1999, The Royal Society.

## APPENDIX A: DE-NOISING OF SIGNALS ARISING IN EXTRA-CORPOREAL SHOCKWAVE LITHOTRIPSY

The following is a further example from acoustical metrology of the potential use of wavelets for de-noising a transient signal.

Extra-corporeal shockwave lithotripsy (ESWL) is an established method for the treatment of kidney stones (renal calculi). In this method, a high amplitude ultrasonic pulse (typically with a "centre" frequency of about 200 kHz) is focused onto the kidney stones of a patient sitting in a water bath. The focusing of the acoustic field and the nonlinear propagation of the wave along the water/tissue path creates a highly distorted shock-wave which fragments the acoustically-hard calculi with no damage to the surrounding tissue (except occasional minor bruising). Following the lithotripsy the calculi may then be passed normally without the need for invasive surgery.

Concern regarding the acoustic output levels of medical ultrasonic equipment has led to regulation requiring that the output be measured to ensure that it falls within safe limits. A robust method for measuring the acoustic output is required to ensure clinical safety, optimise treatment regimes and enable quantitative research and equipment specification. Since at the focus peak pressures can be in excess of 100 MPa, simple hydrophones can easily be damaged during measurements.

At NPL, a velocity interferometer (Figure A.1) has been built to measure the acoustic particle velocity of a target held at the focus of the field produced by a lithotripter. The target is a 3.5 μm thick metal-coated Mylar film stretched over a circular frame. Although optically reflecting, the film is acoustically transparent and moves in sympathy with the acoustic wave. The film is damaged after a number of firings, but is cheap and easy to replace. A bench-top lithotripter source has been developed to provide a test facility that reproduces the fields seen in clinical devices.

A problem with the output of the interferometer is a relatively high noise level. Unfortunately, simple signal averaging of repetitive acquisitions (shots) cannot be used to improve the signal-to-noise ratio since the output of the source varies from shot to shot both in terms of its frequency content and signal amplitude, the variation being partly due to component degradation of the lithotripter equipment. Digital filtering using Fourier based methods is an option, but these tend to reduce unacceptably the high frequency content of the signals. Much information is actually contained in the shock-front (the steep rising edge of the pulse) and standard filtering techniques may degrade this part of the signal, effectively increasing the measurable rise-time (see below). This provides the motivation to investigate the use of wavelet techniques to de-noise the signal without degrading the rise time of the signal.

Figure A.2 shows a typical signal obtained from the interferometer. The result of de-noising the signal using a Fourier-based filtering approach is shown in Figure A.3. The approach involves finding the discrete Fourier transform of the signal, setting to zero high frequency components, and performing the inverse discrete Fourier transform to reconstruct a de-noised version of the signal. The lower graph in the figure shows the residual deviations between the original and Fourier de-noised signals. It is clear that the amplitudes of these deviations are reasonably consistent except in the neighbourhood of the shock where there are residuals that are large in absolute value. This suggests that the shock is not well preserved in the de-noised signal.

Another way to de-noise the signal is to use wavelets. Figure A.4 shows the reconstructed details and level 5 approximation from the DWT of the signal using the *db*4 wavelet. The "standard" de-noising method described in Section 3.2 involves thresholding the detail coefficients followed by reconstruction. However, for this type of signal, where it is important to preserve the steep rising edge, a different approach is applied which exploits the "localisation" properties of the wavelet basis functions. The reconstructed level 1 and 2 details are interpreted as high frequency noise in the signal and the corresponding coefficients are set to zero. The high amplitude parts of the reconstructed details at levels 3, 4 and 5 clearly describe the shock in the signal, whereas the low amplitude parts are also interpreted as noise. For each of levels 3, 4 and 5, the coefficients identified with the shock are therefore retained while all other coefficients are set to zero. The de-noised signal is then reconstructed from the level 5 approximation coefficients and the new detail coefficients.

Figure A.5 shows a de-noised version of the signal obtained using a wavelet-based filtering approach and the residual deviations between the original and wavelet de-noised signals. The plot of the residuals shows that the shock is preserved much better than in the Fourier de-noised signal. Figure A.6, which shows a portion of the original and de-noised signals in the vicinity of the steep rise, illustrates more clearly the difference between the two de-noised signals.

The filtering of the signal based on wavelets is successful because the basis functions are "localised". This property is exploited to retain certain high frequency components in the neighbourhood of the shock and, consequently, to preserve the feature in the de-noised signal. In contrast, the basis functions in a Fourier based method are "global" and it is not possible to simultaneously remove high frequency components and preserve the shock in the de-noised signal.

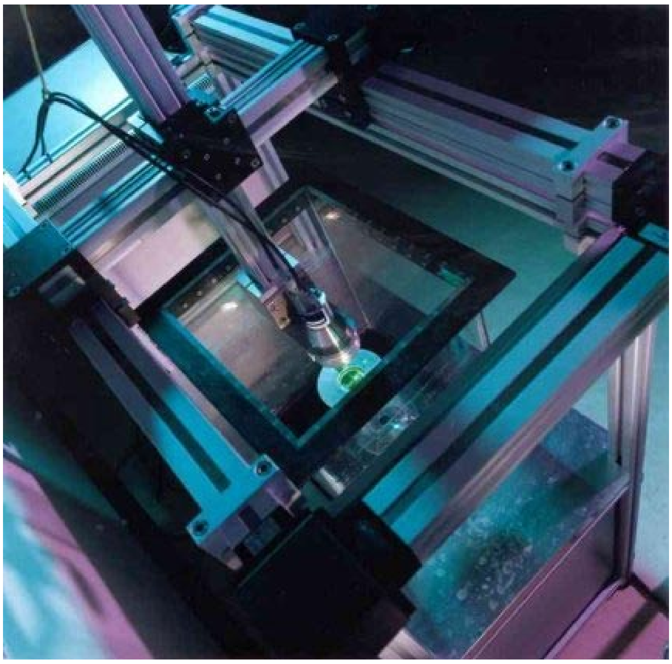

**Figure A.1**: The NPL velocity interferometer used to measure and characterise the shock waves generated in water by extra-corporeal shock-wave lithotripter.

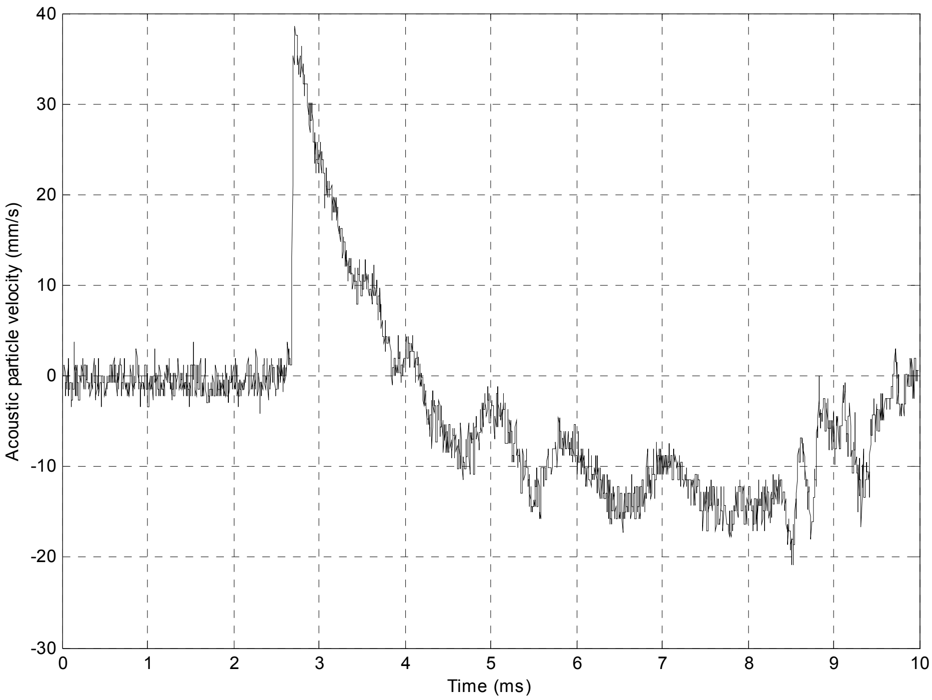


**Figure A.2**: Part of a signal acquired by the velocity interferometer showing the acoustic pulse containing rapid initial rise time and contaminated by background noise. The signal fluctuation occurring after about 4.65 ms is due to *cavitation* in the water and is not part of the acoustic pulse.

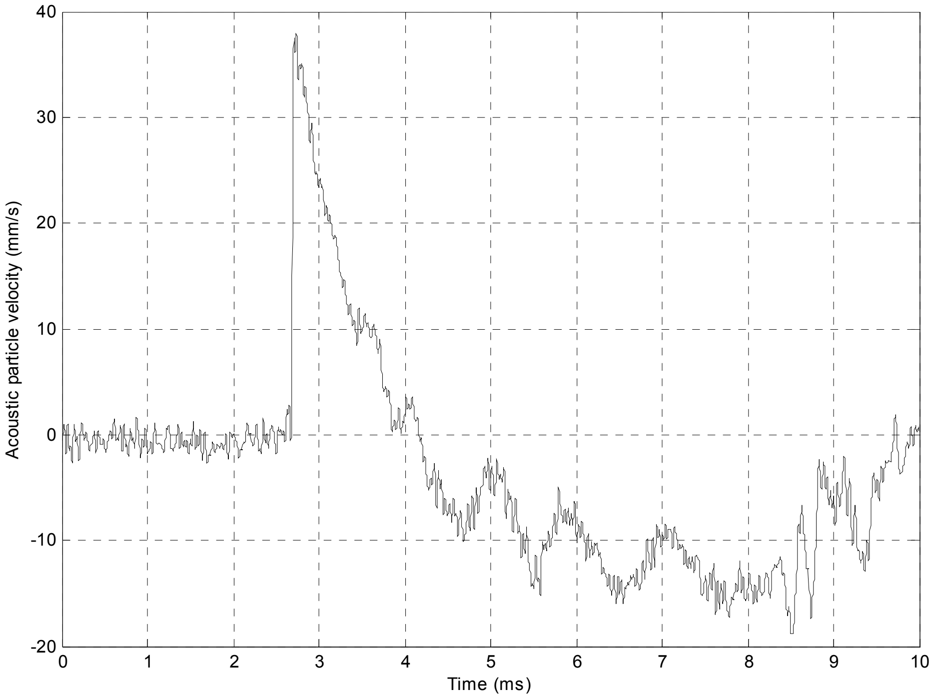


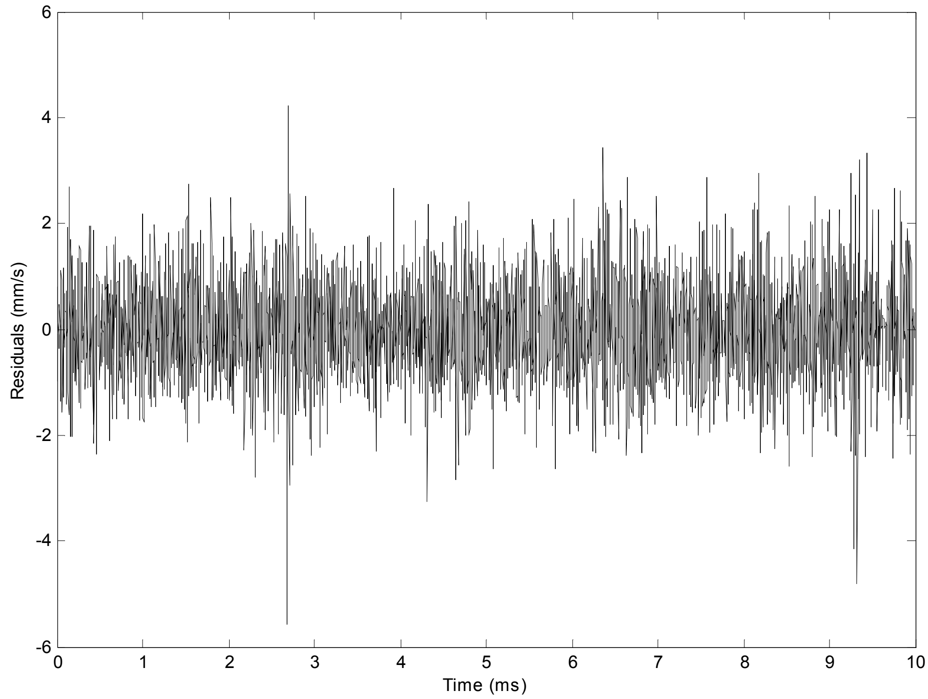


**Figure A.3**: Signal de-noised using the Fourier transform of the signal, and the residual deviations between the original and de-noised signals.

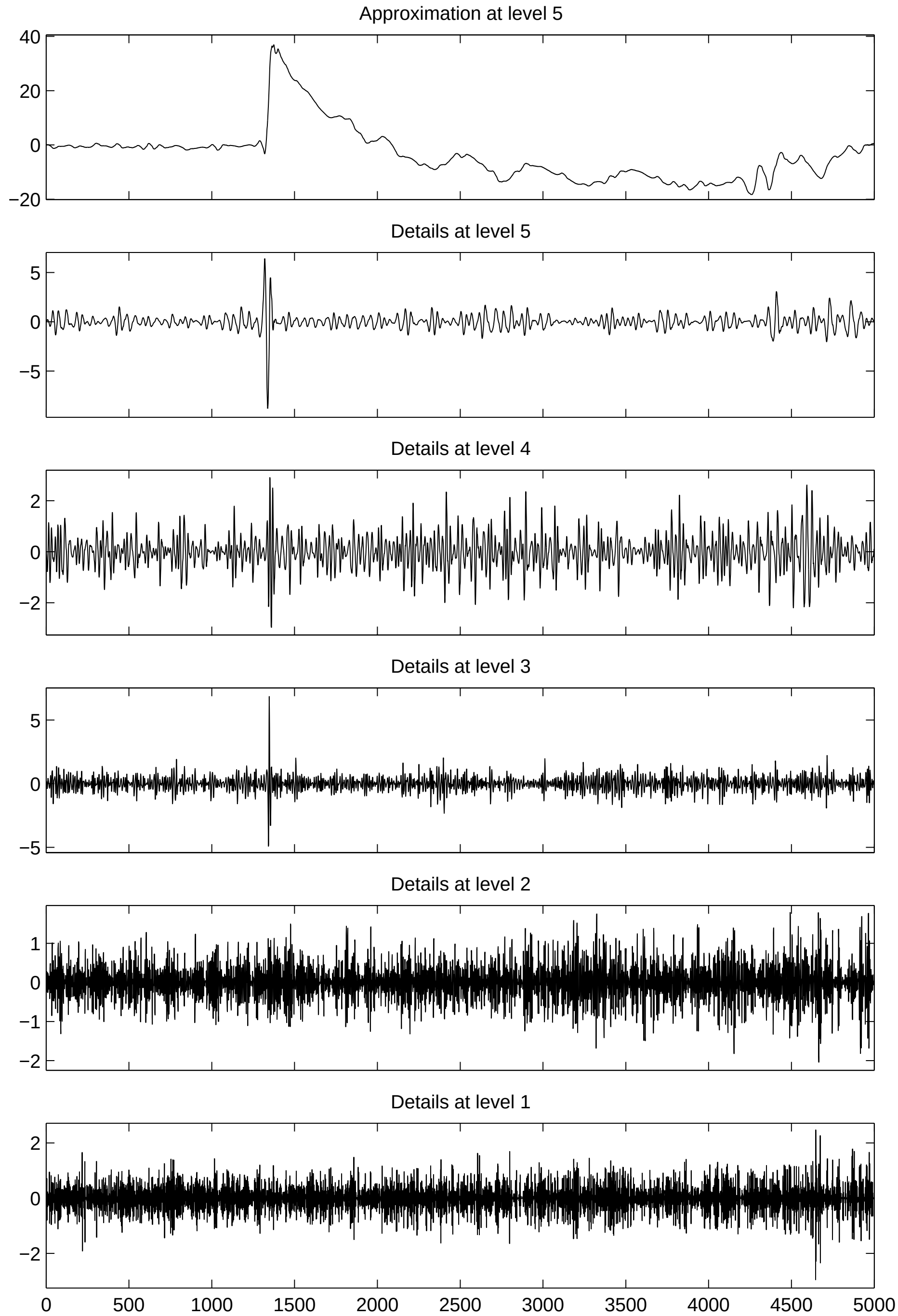


**Figure A.4**: Reconstructed details and level 5 approximation for the signal from Figure A.2. The wavelet for the DWT is *db*4.

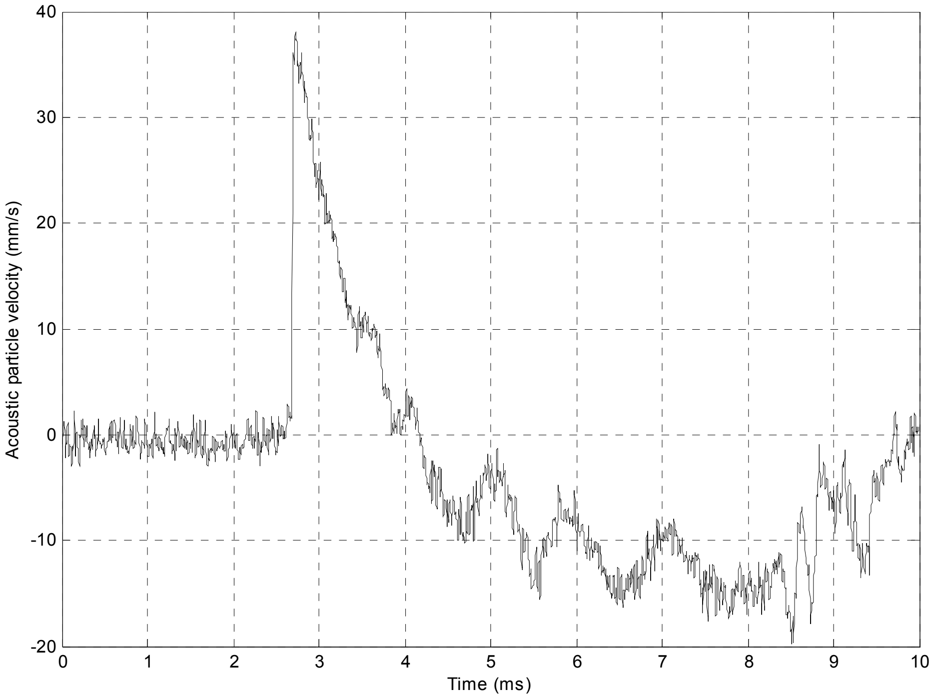


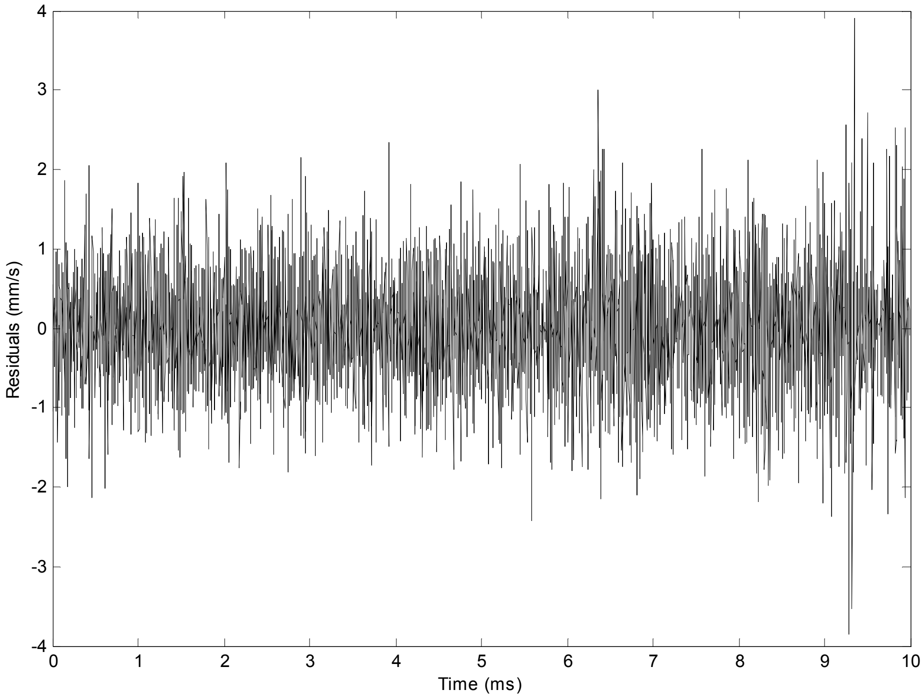


**Figure A.5**: Signal de-noised using wavelets (*db*4, level 5 approximation), and the residual deviations between the original and de-noised signals.

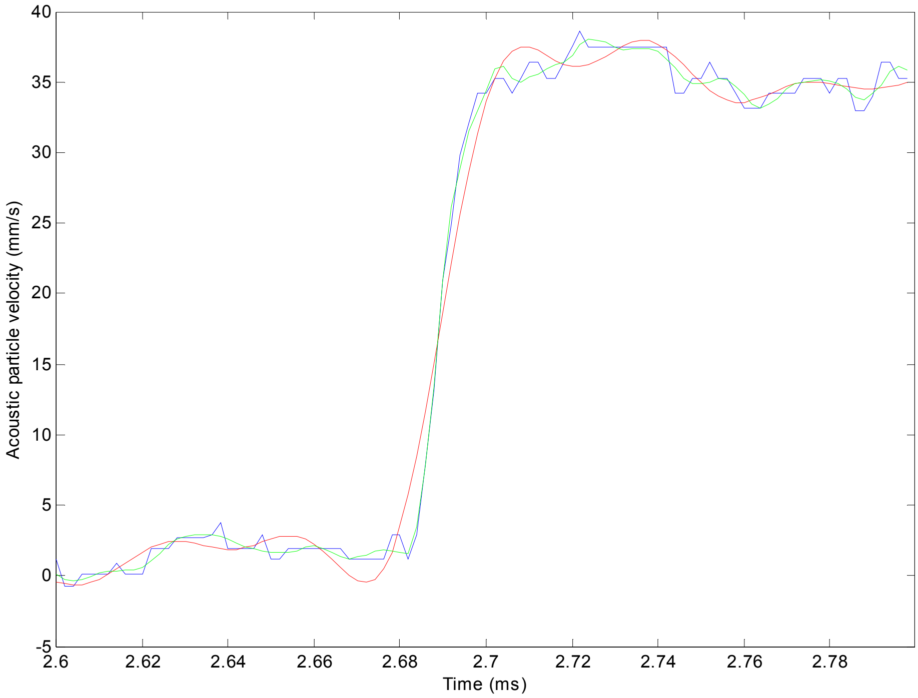


**Figure A.6**: Comparison of the signal de-noising using Fourier and wavelet analysis: portion of the original signal (blue) between 2.6 ms and 2.8 ms, Fourier de-noised (red) and wavelet de-noised (green).